



This is a repository copy of *Compression after multiple low velocity impacts of NCF, 2D and 3D woven composites*.

White Rose Research Online URL for this paper:
<http://eprints.whiterose.ac.uk/150677/>

Version: Accepted Version

Article:

Saleh, M.N., El-Dessouky, H.M. orcid.org/0000-0003-0715-5075, Saeedifar, M. et al. (3 more authors) (2019) Compression after multiple low velocity impacts of NCF, 2D and 3D woven composites. *Composites Part A: Applied Science and Manufacturing*, 125. ISSN 1359-835X

<https://doi.org/10.1016/j.compositesa.2019.105576>

Article available under the terms of the CC-BY-NC-ND licence
(<https://creativecommons.org/licenses/by-nc-nd/4.0/>).

Reuse

This article is distributed under the terms of the Creative Commons Attribution-NonCommercial-NoDerivs (CC BY-NC-ND) licence. This licence only allows you to download this work and share it with others as long as you credit the authors, but you can't change the article in any way or use it commercially. More information and the full terms of the licence here: <https://creativecommons.org/licenses/>

Takedown

If you consider content in White Rose Research Online to be in breach of UK law, please notify us by emailing eprints@whiterose.ac.uk including the URL of the record and the reason for the withdrawal request.



eprints@whiterose.ac.uk
<https://eprints.whiterose.ac.uk/>



This is a repository copy of *Compression after multiple low velocity impacts of NCF, 2D and 3D woven composites.*

White Rose Research Online URL for this paper:
<http://eprints.whiterose.ac.uk/150677/>

Version: Accepted Version

Article:

Saleh, MN, El-Dessouky, HM orcid.org/0000-0003-0715-5075, Saeedifar, M et al. (3 more authors) (2019) Compression after multiple low velocity impacts of NCF, 2D and 3D woven composites. *Composites Part A: Applied Science and Manufacturing*, 125. ISSN 1359-835X (In Press)

<https://doi.org/10.1016/j.compositesa.2019.105576>

Reuse

Items deposited in White Rose Research Online are protected by copyright, with all rights reserved unless indicated otherwise. They may be downloaded and/or printed for private study, or other acts as permitted by national copyright laws. The publisher or other rights holders may allow further reproduction and re-use of the full text version. This is indicated by the licence information on the White Rose Research Online record for the item.

Takedown

If you consider content in White Rose Research Online to be in breach of UK law, please notify us by emailing eprints@whiterose.ac.uk including the URL of the record and the reason for the withdrawal request.



eprints@whiterose.ac.uk
<https://eprints.whiterose.ac.uk/>

1
2
3
4 Compression After Multiple Low Velocity Impacts of NCF, 2D and 3D Woven
5
6 Composites

8 Mohamed Nasr Saleh^{a,1*}, Hassan M. El-Dessouky^{b,c,1*}, Milad Saeedifar^a, Sofia Teixeira De
9 Freitas^a, Richard J. Scaife^b, Dimitrios Zarouchas^a

11 ^a Structural Integrity & Composites, Faculty of Aerospace Engineering, Delft University of
12 Technology, Delft, 2629 HS, The Netherlands

13 ^b Composite Centre, AMRC with Boeing, University of Sheffield, Rotherham S60 5TZ, UK

14 ^c Physics Department, Faculty of Science, Mansoura University, Mansoura 35516, Egypt

15 ¹ Contributed-equally

16 * Corresponding authors: m.a.s.n.saleh@tudelft.nl & h.el-dessouky@sheffield.ac.uk

27 **Abstract**

28
29
30 This paper investigates the effect of the fabric architecture and the z-binding yarns on the
31 compression after multiple impacts behavior of composites. Four fiber architectures are
32 investigated: non-crimp fabric (NCF), 2D plain weave (2D-PW), 3D orthogonal plain (ORT-
33 PW) and twill (ORT-TW) weave. The specimens were subjected to single and multiple low-
34 velocity impacts at different locations with the same energy level (15 J). Non-destructive
35 techniques including ultrasonic C-scanning, X-ray CT and Digital Image Correlation (DIC) are
36 employed to quantitatively analyze and capture the Barely Visible Impact Damage (BVID)
37 induced in the specimens. Although the absorbed energy was approximately the same, damage
38 was the least in 3D woven architectures. In the case of compression after impact, 3D woven
39 composites demonstrated a progressive damage behavior with the highest residual strength
40 (~92%) while 2D plain weave and NCF specimens showed suddenly catastrophic damage and
41 the residual strength of ~65% and ~55% respectively.

42 Keywords: A. 3-Dimensional reinforcement; B. Impact behaviour; B. Damage tolerance; D.
43 Non-destructive testing; Repeated impact

1 Introduction

Fiber-reinforced composites are widely used in automotive, oil and gas, aerospace and wind energy industries nowadays thanks to their high strength and stiffness to weight ratio compared to traditional metals. Two-dimensional (2D) composites, made of unidirectional or woven plies, are the most popular types used in industrial applications. Although they possess relatively high strength and stiffness in the in-plane direction, they are characterized by poor transverse “out-of-plane” properties especially when subjected to impact loading. It does not require high velocity impacts to induce severe internal damage into such 2D composite laminates. Thus, Low Velocity Impacts (LVI) has been a serious threat to their use in real life applications as they cause Barely-Visible Impact Damage (BVID). BVID, in fiber-reinforced composites, is one of the most critical damages in different industries, such as aerospace [1], maritime [2] and oil and gas [3], as it can go undetected while causing a significant, more than 50% [4], degradation that might lead to catastrophic failure. Generally, composite structures, such as aircrafts and composite pipes for instance, are susceptible to LVI during maintenance or ground handling. These impacts can happen because of tools dropping or support-trucks accidents, for instance. According to a report published by Boeing [1], three major causes resulted in most of the repairs for the Boeing 747 fuselage in the course of its service life. These were fatigue cracks (57.6 %), corrosion (29.4 %) and impact damage (13.0 %). Impact induced damage leads to matrix cracking, delamination, fiber matrix debonding and fiber breakage leaving only small indents on the impacted surface. To mitigate such problems, large safety margins are usually introduced in the design process of composite components and structures, which in return reduces significantly their competence with metals. With the advancement in the technical textile and weaving industries, three-dimensional (3D) woven composites have been introduced as an alternative to 2D composites whereby the out-of-plane properties are improved. Thanks to their unique characteristic of through-thickness reinforcement in resisting the delamination and transverse matrix cracking growth [5–9], 3D woven composites have been recently used in aerospace industry in as subcomponents for engines and landing gears [10,11] and potentially demonstrated for automotive applications [12].

To quantify the performance of composite materials in the out-of-plane loading, two conventional indicators are defined. The first is the impact resistance of the composite material characterized by the absorbed energy and the level of induced damage due to a specific impact

1
2
3
4 energy. The second is the damage tolerance, defined as the ability to maintain the undamaged or
5 initial strength and quantified by measuring their residual strength [11] after impact in tension
6 (TAI), compression (CAI) and flexure (FAI). Shah et al. [11] classified the various factors
7 affecting the impact resistance and damage tolerance of composite materials into primary and
8 secondary ones, based on the significance of their effect. The primary factors are the fabric
9 architecture and the resin toughness. The secondary factors include, but not limited to:
10 environmental conditions, stacking sequence, impactor geometry and repeated impacts.
11
12
13
14
15
16
17

18 Several studies investigated the impact resistance of unidirectional (UD) [4], non-crimp
19 fabric (NCF) [13], 2D [14,15] and 3D [8,14,15] woven composites subjected to LVI. In the case
20 of 2D laminated composites, some researchers [16,17] tried to optimize the stacking sequence to
21 improve the impact resistance by improving the interlaminar fracture toughness. They concluded
22 that by changing the stacking sequence, interlaminar fracture can be suppressed or delayed by
23 changing the load from tensile to compressive between the plies. For 3D woven composites
24 [15,18], the through thickness reinforcement was found to increase the delamination resistance
25 due to impact as well as energy absorption compared to their 2D counterparts. Besides, by
26 changing the properties of the through-thickness yarns, the performance can be significantly
27 improved. Damage tolerance of UD [16,19], NCF [20], 2D and 3D woven composites [14,15,19]
28 were investigated via CAI, TAI and FAI testing. Potluri et al. [19] studied the effect of fabric
29 architecture on the damage tolerance under CAI loading. They compared UD, 2D and 3D woven
30 composites. They concluded that 3D woven composites demonstrated the highest residual
31 strength, but they also observed that there is a critical damage size below which there is no
32 significant difference in the residual strength for 3D woven composites. Hart et al. [15]
33 compared the residual strength of 2D vs. 3D woven composites using CAI and FAI testing. Two
34 main remarks were made. The first was that the 3D woven composites had the least reduction in
35 strength due to the z-binding yarns suppressing delamination growth. The second was that FAI
36 could be an attractive alternative testing approach to CAI as the reduction of strength due to
37 impact was better captured. In other words, FAI was found to be more sensitive to delamination
38 and damage due to impact compared to CAI. This could be attributed to the size of the impacted
39 region compared to the specimen dimensions and the nature of the load in flexure being more
40 dependent on the load-bearing element “fibers” in the tested composites.
41
42
43
44
45
46
47
48
49
50
51
52
53
54
55
56
57
58
59
60
61
62
63
64
65

1
2
3
4 With less work [1–3,21–24] focusing on the effect of repeated impacts on the residual
5 strength of fiber-reinforced composites, most of researchers investigated only the repeated
6 impacts occurring at the same location. Baucom et al. [24], for instance, compared the effect of
7 repeated impacts on various fabric architectures including 2D and 3D composites. They observed
8 that 3D woven composites absorb more energy and distribute the damage on a larger area in the
9 form of matrix cracking and fiber-matrix debonding. While in the case of 2D composites,
10 dominant damage mechanisms were matrix cracking, excessive delamination and fiber breakage.
11
12
13
14
15
16
17

18 From an application point of view, repeated impacts might occur to the same composite
19 structure but at different locations, which, to the authors' knowledge, has not been thoroughly
20 investigated in the literature. Thus, the motive for this study is to simulate multiple impacts with
21 the same energy level at different locations for different composite architectures and study their
22 effect on the residual strength in CAI. An extensive experimental campaign is, thus, developed to
23 compare the single vs. multiple impact response of two 2D laminated composites, represented by
24 NCF and 2D plain woven architectures, as well as two 3D woven composites, represented by
25 orthogonal plain and twill architectures, as described in Section 2. Section 3 details the
26 experimental procedure for both single and multiple impact testing, the use of NDT techniques
27 such as ultrasonic C-scanning and X-ray computed tomography (CT) to quantify the level of
28 induced damage and the residual strength determination using the CAI testing. Then, the
29 discussion of the impact and CAI responses, for the four tested architectures, is reported in
30 section 4. The comparison of the four fabric architectures is based on their response to single vs.
31 multiple impact, the impact resistance, their damage tolerance and failure nature. Finally, section
32 5 provides a summary of the main concluding remarks of this study.
33
34
35
36
37
38
39
40
41
42
43
44
45
46

47 **2 Materials and manufacturing**

48 **2.1 Materials and architectures' design**

49
50 A recently developed weave-design software (EAT-3D Composites Module) for
51 technical weaving and complex composite structures was used to design the 2D plain (2D-PW),
52 3D orthogonal plain (ORT-PW) and twill (ORT-TW) weaves; each of which consists of 5 warp
53 and 5 weft layers, including the z-binding yarns in the warp. All weaves were designed with the
54 same drafting plan to weave fabrics with the same loom setup and just change weave designs
55
56
57
58
59
60
61
62
63
64
65

1
2
3
4 from one preform to the other. Fig. 1 demonstrates the unit-cell schematic of the four different
5 fabrics investigated in this study. The unit-cell is defined as the smallest volume element that can
6 represent the composite constituents, geometrical features and yield homogenized properties
7 representative for the whole structure. The main difference between the two 3D orthogonal
8 weaves is the z-binding yarn's path, which directly affects the unit-cell size of the weave. In the
9 case of the ORT-PW (Fig. 1c), the binding frequency, through the thickness, is twice the binding
10 frequency of the ORT-TW (Fig. 1d). The effect of the unit-cell size on the impact resistance and
11 CAI response is discussed in section 4.
12
13
14
15
16
17
18

19 A modified Dornier double-*rapier* FT-Dobby loom was used to produce the 2D and 3D
20 weaves. A creel of 1100 positions was loaded with T700-12k carbon fiber bobbins to warp the
21 loom. The creel was equipped with tension system to control the tension of warp and binder
22 during the weaving process. To produce a balanced fabric, the densities of the warp and the weft
23 were set to be the same: 12.66 ends/cm and 12.66 picks/cm respectively. Five layers of the 2D-
24 PW architecture (Fig. 1b) were woven simultaneously, and 5 layers of the NCF (Fig. 1a) were
25 used so that all produced fabrics have approximately the same areal density (~2000 GSM).
26
27
28
29
30
31
32

33 **2.2 Composite panels manufacturing**

34 A resin transfer molding (RTM) tool of 500 mm x 500 mm, manufactured by Composite
35 Integration Ltd., was used to manufacture flat composite panels. The laminate thickness was
36 designed to be ~2.5 mm to achieve ~50 % fiber volume fraction for all the architectures. The
37 matrix used was Gurit T-Prime 130-1 having a mixing ratio of 100/27 by wt% of resin/hardener.
38 The tool was preheated to 80 °C. The resin was degassed before injection in a degassing chamber
39 for 30 minutes, and then placed in a pressure pot. The injection occurred at 2 bars of pressure,
40 and -1 bar of vacuum. Upon fully wetting the preform the outlet was clamped. The pressure was
41 left on for 15 minutes to ensure the entire mold had an even pressure and to reduce voids content
42 in the final composite, if any. The panels were left to cure, in the RTM tool, for 1 hour at 80 °C.
43
44
45
46
47
48
49
50
51
52
53
54
55
56
57
58
59
60
61
62
63
64
65

3 Experiment and characterization

3.1 Impact testing

The testing setup to produce the BVID in the different specimens' architectures is described in this section. Three repeats from each type were used in all tests. Moreover, the reasoning behind the research approach for multiple impacts using the same energy level is discussed.

3.1.1 Single impact

Impact testing for all specimens was conducted using a drop-weight tower as per the ASTM D7136 "Standard Test Method for Measuring the Damage Resistance of a Fiber-Reinforced Polymer Matrix Composite to a Drop-Weight Impact Event" [25]. Specimens were clamped using the impact support fixture designed based on the ASTM standard to have a cut-out of 125 ± 1 mm in the length direction and 75 ± 1 mm in the width direction. The SI units version of the ASTM D7136 is used for all specimens (see Fig. 2). For the first set of specimens, they were all impacted in the center, with a hemi-spherical impactor with a diameter of 16 mm and a mass of 4 kg, as depicted in Fig. 2a. As the scope of this study is the LVI, the impact energy was determined based on the maximum that the weakest architecture "NCF" can accommodate without reaching the perforation threshold. Higher energies such as 25, 20 and 18 J were investigated experimentally before reaching the final decision of using 15 J as the impact energy for this study.

3.1.2 Multiple impact

The motive for this section is to simulate multiple impacts with the same energy level on the different composite architectures and study their effect on the residual strength in compression. To achieve this, a second set of specimens "three of each" were impacted twice (left and right), 25 mm apart from the first impact (see Fig. 2b) with the same impactor and the same energy. The locations of the 2nd and 3rd impacts were determined in a sense to avoid any overlap between the individual impacts as the impactor diameter was 16 mm. Moreover, they were chosen to avoid any boundary effect due to the clamping fixture. As the same impact support fixture was used, the boundary conditions for the 2nd and 3rd impacts were different from the 1st impact. Detailed analysis of the effect of the boundary conditions during impact testing can be found in [14]. This change of boundary conditions due to clamping could have an effect

1
2
3
4 on the depth of dent, the stiffness of the load-displacement curves and the damage area which
5 will be discussed further in section 4.1.3. For all the conducted impacts, either single or
6 multiple, the impact tower was equipped with a rebound catcher (see Fig. 3b) to ensure that the
7 impactor strikes the specimen only once.
8
9

10 11 12 **3.2 Ultrasonic C-scanning**

13
14 Before carrying out the CAI testing for the single and multiple impacted specimens,
15 ultrasonic C-scanning was used as a Non-Destructive Technique (NDT) to evaluate the level of
16 induced damage due to impact and to provide more information about the resistance against
17 damage growth of the different architectures of interest in this study. The system used to scan the
18 impacted specimens is a Midas NDT system with Zeus software. It has one transmitter and one
19 receiver transducers with a frequency of 10 MHz, and the specimens were placed in-between.
20 The scanning speed used was 200 mm/min.
21
22
23
24
25
26
27

28 **3.3 X-ray Computed Tomography (CT)**

29
30 To evaluate the level of internal damage due to impact loading, X-ray CT scans were
31 performed for the different types of impacted specimens using a Nikon XTH-320 machine. The
32 225 kV source with reflective target was used with a 0.125 mm copper filter. The total volume in
33 the field of view was $22.5 \times 19 \times 5.5 \text{ mm}^3$, resulting in a resolution of $\sim 13.2 \text{ }\mu\text{m}$. The source
34 voltage and current were set to 220 kV and 59 μA respectively. The exposure time for each
35 radiograph was ~ 1.4 seconds, with 3142 radiographs being collected over 360° . The total data
36 acquisition time was ~ 1.25 hours. After scanning, the raw data was used to reconstruct the 3D
37 volume using VGSTUDIO MAX software.
38
39
40
41
42
43
44

45 **3.4 CAI testing**

46
47 CAI testing for all specimens was conducted according to the ASTM D7137 “Standard
48 Test Method for Compressive Residual Strength Properties of Damaged Polymer Matrix
49 Composite Plates” [26]. The test set up is shown in Fig. 3d. For baseline comparison, non-
50 impacted specimens from each architecture were tested in compression using the same test setup.
51 For the impacted specimens as previously highlighted, there were two sets of CAI testing. The
52 single-impacted specimens (see Fig. 3a) were directly tested in compression after the first single
53 impact (see Fig. 3d). However, the multiple-impacted specimens were tested in compression (see
54 Fig. 3d) after going through the process of three impacts as depicted in Fig. 3a-c. The impacted
55
56
57
58
59
60
61
62
63
64
65

1
2
3
4 specimens were loaded in compression with a displacement-controlled crosshead of 1.25
5 mm/min while being supported by the CAI fixture to minimize loading eccentricities and any
6 induced specimen's bending. The crosshead displacement and the applied force were recorded
7 using a 500 kN load-cell MTS 810 hydraulic testing machine. Three-dimensional (3D) Digital
8 Image Correlation (DIC) system (see Fig. 3d) was calibrated and used to capture the
9 displacement contour map during the test. The DIC system used for the full-field strain
10 measurement consisted of two 8-bit "Point Grey" cameras with "XENOPLAN 1.4/23" lenses.
11 Both cameras had a resolution of 5 MP. ViC-Snap 8 software was used to record the speckle
12 pattern images with an acquisition rate of 2 frames per second (fps). Then, the acquired images
13 by ViC-Snap 8 were processed using ViC-3D 8 software. For processing, the subset size was set
14 to 100 x 100 pixels with a step size (distance between subsets) of 7 pixels. The observation
15 window of approximately (120 x 70) mm² produced an image with dimensions of (2048 x 1194)
16 pixels.
17
18

19 In addition to using the 3D DIC system during the CAI test, it was utilized before the test
20 to measure the dent depth for all types of specimens for both the single and multiple impacted
21 cases. On average, 15 images were captured with the Vic Snap 8 software, and then processed
22 with the same aforementioned parameters using ViC-3D 8 software. Detailed comparison of the
23 dent depth is discussed in section 4.1.
24
25
26
27
28

29 **4 Results and discussion**

30 **4.1 Impact testing**

31 Results from the ultrasonic C-scanning for both single and multiple-impacted specimens,
32 DIC dent depth measurements, impact load-displacement response and the energy absorption are
33 detailed in this section.
34
35
36
37
38

39 **4.1.1 Single Impact**

40 After the first impact, the C-scan (Fig. 4) shows a clear difference for the impact damage
41 among the four architectures. The shape of the damaged area is one of the main differences. In
42 the case of the NCF, where there is minimal waviness in the architecture, the damage area has a
43 cross (0°/90°) shape. The splitting in the 0° layers is due to the longer floats compared to the 90°
44 counterpart as previously reported in [27]. Moreover, the NCF specimens are characterized by
45
46
47
48
49
50
51
52
53
54
55
56
57
58
59
60
61
62
63
64
65

1
2
3
4 the largest damage area. This cross shape of the damaged area almost vanishes in the case of the
5
6 2D-PW, with again a relatively large damage compared to the 3D woven counterparts. For both
7
8 the ORT-PW and ORT-TW, the damaged area is smaller than the NCF and 2D-PW cases with
9
10 the ORT-PW having the least damaged area. Using the 3D DIC system to calculate the dent
11
12 depth suggests that the depth because of the first impact is almost the same for all architectures.
13
14 This can be attributed to the fact that the energy absorption for all the architectures is almost the
15
16 same as discussed later in section 4.1.3.

17 18 **4.1.2 Multiple Impact**

19
20 For the multiple-impacted specimens, the C-scan (Fig. 5) revealed more information
21
22 about the nature of the damage occurred due to the three impacts. In the case of the NCF
23
24 specimens, it is again clear that the splitting along the longitudinal direction is larger than the
25
26 transverse one. In addition, the three damaged areas are interconnected. This suggests that
27
28 delamination propagated in the width direction, as well, causing the NCF to suffer from the
29
30 largest damaged area. For the 2D-PW case, the damage propagated more in the longitudinal
31
32 direction than the transverse one. Due to the waviness of the individual plies, the damaged area
33
34 did not grow as much as the NCF case. Thanks to the existence of the z-binding yarns in the 3D
35
36 woven composites, the damaged area is localized and no interconnection between the three
37
38 impacted regions occurred. The dent depth calculations, using the 3D DIC, revealed that the
39
40 NCF specimens do not only have the largest damage area, but also the deepest dent. Detailed
41
42 quantitative comparison between the single and multiple impact dent depth is discussed in the
43
44 following section.

45 46 **4.1.3 Single vs. multiple impact**

47
48 Following the discussion in the previous sections, a detailed comparison between the
49
50 single and multiple impact cases can be described based on: i) the impact load-displacement
51
52 response, ii) the energy absorption and damage area calculated from the C-scans, iii) the internal
53
54 damage captured by X-ray CT and iv) the dent depth measured using the DIC system.

55
56 Representative impact load-displacement curves obtained from the weight-drop impact
57
58 tower for the three impacts are summarized in Fig. 6 for all the architectures. As a general
59
60 remark, the effect of the clamping boundary conditions due to the clamping fixture “specimens’
61
62 holder” is clear when comparing the stiffness of the load-displacement curve of the first impact
63
64
65

1
2
3
4 with the other consequent impacts. As the first impact occurs in the middle of the specimen, it
5 undergoes more deflection for the same load level compared to the other two adjacent impacts.
6 This therefore results in lower stiffness and larger deformation, regardless of the architecture of
7 the impacted specimens. When it comes to the NCF specimens (see Fig. 6a), two important
8 observations can be made. The first is regarding the maximum load being the least among all the
9 other architectures. The second is regarding the maximum deformation being the largest among
10 them. This, combined with the previous discussion about the amount of damage induced in the
11 NCF specimens due to impact, emphasizes the inferiority of laminated (NCF) composites in
12 sustaining the out-of-plane loading. For the other architectures, either 2D (Fig. 6b) or 3D (Fig.
13 6c,d) woven composites, this level of impact energy (15 J) did not cause a significant difference
14 in their response from the load-displacement point of view.
15
16
17
18
19
20
21
22
23
24

25 For the sake of understanding the effect of the composite's architecture on the impact
26 resistance, it is quite common to analyze the load-displacement response in the light of the
27 damage-induced area and the energy absorbed by the impacted specimen. Thus, Table 1 details
28 the level of the induced damage as a percentage of the total area of the specimen, for each
29 architecture, calculated using MATLAB image segmenter. The trend is quite similar in the case
30 of the single-impacted and multiple-impacted specimens. The NCF specimens experience the
31 largest damage, followed by the 2D-PW, with the ORT-PW having the least damage. This
32 confirms what previous studies [28–33] suggested regarding the role of the z-binding yarns in
33 resisting delamination growth in 3D woven composites for different loading conditions. This is
34 supported by the X-ray CT slices reported later in this section.
35
36
37
38
39
40
41
42
43

44 Figure. 7a represents a typical energy vs. time impact curve [27]. It defines the
45 difference between the elastic and absorbed energy due to impact loading. The energy is
46 calculated as the integration of the load-displacement curve. Moreover, Fig. 7b compares the
47 absorbed energy for all architectures after the first impact as well as the total absorbed energy
48 after the three impacts. NCF specimens are characterized by the highest stiffness, due to the least
49 crimp and the straightness of the fibers, compared to the 2D and 3D woven architectures.
50 Consequently, their energy absorption was the highest with ~14 and 42 J respectively. For 2D-
51 PW, ORT-PW and ORT-TW, the energy absorption was almost the same with ~ 13 and 38 J
52
53
54
55
56
57
58
59
60
61
62
63
64
65

1
2
3
4 respectively. Therefore, in spite of the comparable absorbed energy, the difference in the induced
5 damage is significant, with 3D woven composites resisting the most.
6
7

8
9 Generally, LVI results in internal damage such as matrix cracking, fiber damage and
10 fiber-matrix debonding. As discussed by Shah et al. [11], the level of damage caused by LVI
11 depends on two primary factors including the fabric architecture and resin toughness. The resin
12 toughness factor is outside the scope of this study. Nevertheless to further understand the role of
13 fabric architecture and the z-binding yarns in delamination and impact resistance, cross-sectional
14 slices from the X-ray CT reconstructed volume are analyzed. Figure 8 depicts a cross-sectional
15 slice along the warp (0°) direction, right at the location where the impactor strikes the specimen.
16 Although the impact energy was relatively low and caused only BVID on the surface, X-ray CT
17 slices reveal excessive delamination at the impacted region. In the case of NCF specimens (see
18 Fig. 8a), delamination between plies, highlighted in red, spans the full width of the field of view.
19 Moreover, the fracture of the back side of the specimen, because of the impact, indicates fiber
20 breakage in the bottom-most plies. For 2D-PW specimens (see Fig. 8b), delamination is a bit
21 suppressed, compared to the NCF case, due to the waviness of the plies being 2D plain woven;
22 but it is still guided by this waviness between the plies. In the aforementioned cases, the
23 delamination resistance is only a function of the toughness of the matrix or the plies' waviness.
24 On the contrary, in the case of 3D woven composites (see Fig. 8c,d) delamination is arrested by
25 the z-binding yarns. Comparing the ORT-PW (Fig. 8c) with ORT-TW (Fig. 8d), it can be
26 concluded that the higher the frequency of the z-binding yarn in the through thickness direction
27 "the smaller the unit-cell size", the less the delamination propagation due to impact. Another
28 damage mechanism can also be observed in these two cases in the form of matrix cracking in the
29 resin-rich regions, which has been reported in [34,35] as one of the drawbacks of 3D woven
30 composites. Matrix cracking and delamination in the case of ORT-TW are more noticeable
31 compared to their ORT-PW counterparts (see Fig. 8c, d). They can grow longer because the
32 distance enclosed by the z-binding yarn "L" is almost twice the distance in the ORT-PW case.
33 However in both cases, once they reach a z-binding yarn, the damage mechanism changes to a
34 different type, which is referred to here as binder-guided delamination. The energy required to
35 break the reinforcing z-binding yarn is higher than the energy required for the delamination or
36 the matrix cracking to alter its direction. Once the energy of the impact is sufficient to break the
37 z-binding yarn, like in the case of the ORT-TW (Fig. 8d), the yarn fractures.
38
39
40
41
42
43
44
45
46
47
48
49
50
51
52
53
54
55
56
57
58
59
60
61
62
63
64
65

1
2
3
4 Besides analyzing the first and consequent impacts using the C-scanning and X-ray CT
5 slices, dent depth measurements using DIC can be also valuable. Figure 9 compares the dent
6 depth across the width of the specimen for the single and multiple impact cases. The measured
7 dent depth indicates the level of plastic deformation induced in the impacted specimens.
8 Therefore, the difference among the tested architectures can be analyzed in the light of the
9 specimens' stiffness and accordingly the elastic vs. absorbed energies. The dent depth due to the
10 first impact (Fig. 9a), regardless of the architecture, is very similar with a maximum value of
11 ~0.2 mm as the impact energy is relatively low. However the dent depth, in the case of the three
12 impacts (Fig. 9b), indicates significant dependency on the composite architecture. As a general
13 observation, the side impacts result in a deeper dent compared to the central one. This can be
14 attributed to the previous discussion regarding the effect of the clamping boundary conditions.
15 As expected from the stiffness and energy absorption discussion, the NCF specimens undergo
16 the largest deformation with the highest interaction between the adjacent impacts leading to ~1.4
17 mm side dent depth and ~0.8 mm central dent depth. For the other architectures, the effect is less
18 severe leading to side dent depth of ~0.3mm.

32 4.2 CAI testing

35 4.2.1 Load-displacement response

36 The load-displacement curves for: baseline, single impact and multiple impact specimens
37 are shown in Fig. 10a-c. A clear distinction, between the NCF and 2D-PW from one side and the
38 3D woven composites (ORT-PW and ORT-TW) from the other side, is observed when it comes
39 to the nature of the final failure. For NCF and 2D-PW, baseline and single impact (see Fig. 10 a,
40 b), the failure is more like a catastrophic failure with a sudden drop in the compressive load and
41 a relatively less failure displacement (~1.5 mm). In the case of multiple impact for NCF and 2D-
42 PW (see Fig.10 c), the failure is still catastrophic but the compressive load drops in steps, each of
43 which corresponds to failure occurring in the vicinity of one of the three impacts. On the
44 contrary, the ORT-PW and ORT-TW 3D woven architectures (see Fig. 10 a-c) exhibit a
45 progressive failure response with a gradual drop in the compressive load and a larger
46 deformation indicated by the compressive displacement (~ 3.5 to 4 mm). This directly indicates
47 the importance of the z-binding yarns in 3D woven composites in resisting the internal damage
48 and transforming the failure behavior from a catastrophic to a progressive one.

1
2
3
4 The comparison of the residual strength, for single-impacted and multiple-impacted
5 specimens as function of the baseline strength, is depicted in Fig. 10d. The NCF experiences the
6 largest reduction in the residual strength for the first and the multiple impacts (~20 % & 45 %
7 respectively). For 2D PW, the reduction in residual strength is (~25 % & 35 %) for the single and
8 three impacts. In the case of 3D woven composites and regardless of their unit-cell size, the
9 strength reduction is the least. In addition, it is not much different from the single and the
10 multiple impacts (~8 %). This observation agrees well with the conclusion drawn by Potluri et al.
11 [19] that if the damage size is less than a critical value, there is no noticeable difference in the
12 CAI residual strength of 3D woven composites. The damage, caused by such LVI, in 3D woven
13 composites is very localized and contained within the impact location. The fact that the damaged
14 regions are not interconnected reduces the effect of multiple impact on the residual strength in
15 CAI. This highlights the damage tolerance of 3D woven composites as opposed to their 2D
16 counterparts.
17
18
19
20
21
22
23
24
25
26
27

28
29 In general, fiber-reinforced composites fail in axial compression by kinking of the load-
30 bearing tows. Kinking is a failure process [36] that occurs when the applied compressive stress
31 exceeds a threshold level and induces plastic shear flow of the resin within and surrounding an
32 axial tow. The fibers inside the tow rotate with the increase in the load until the tow becomes
33 unstable and breaks a long a well-defined plane known as a kink band as shown in Fig. 11a. In
34 the case of 2D laminated composites, clusters of kink bands grow simultaneously leading to this
35 observed sudden failure in the load-displacement curves. Moreover due to impact loading of
36 NCF and 2D-PW, excessive delamination growth occurs between the plies creating sub-
37 laminates [4,11,13,19,27]. These sub-laminates then fail due to fiber micro-buckling and kink
38 bands formation as delamination increases the unsupported length and consequently, reduces the
39 load-carrying capacity of the individual plies. In the case of 3D woven architectures, the z-
40 binding yarns play an important role in suppressing delamination due to impact as well as
41 constraining the kink bands formation. Cox et al. [37] investigated the mechanics of compressive
42 damage in 3D woven composites and reported that kink bands formation occurs first in the most
43 severely distorted tows. These tows are normally the surface tows due to the interlacement with
44 the z-binding yarns (see Fig. 11b). Although the surface tows fail, buckling is usually
45 constrained by the z-binding yarn at the interlacement point. Upon increasing the compressive
46 load, more kink bands form in other distorted tows. In other words, formation of kink bands in
47
48
49
50
51
52
53
54
55
56
57
58
59
60
61
62
63
64
65

1
2
3
4 3D woven composites occurs as discrete geometric and sequential flaws rather than simultaneous
5 and sudden formation as their 2D counterparts. As a result, 3D woven composites loaded in
6 compression fail gradually at discrete locations across the whole specimen width leading to the
7 high deformation-to-failure.
8
9

10
11
12 Improving the damage resistance of composite materials, due to the z-binding yarns existence,
13 comes at another cost, which is the ultimate compressive strength in this case. Comparing the
14 ultimate compressive load in the case of the baseline specimens (see Table 2) clearly reflects the
15 effect of crimp in 2D and 3D woven composites. This crimp effect has been the scope of many
16 research studies in the literature [11,28,38–41], and it confirms the trend observed in this study.
17 NCF with the least waviness exhibits the maximum compressive strength (see Table 2), followed
18 by the 2D-PW, then the ORT-TW and the ORT-PW withstanding the least compressive load to
19 failure. Although all architectures are designed to have the same fiber volume fraction in each
20 direction (0° and 90°), the waviness of the 2D-PW leads to the knock-down in strength compared
21 to NCF. In the case of 3D woven composites, the effect of the unit-cell size and the z-binding
22 yarns frequency becomes very significant. The ORT-TW specimens have less crimp and more
23 importantly less stress concentration points at the interlacement point between the z-binding
24 yarns and the in-plane warp and weft yarns compared to the ORT-PW specimens. Thus, the
25 ultimate compressive strength of the ORT-PW specimens is found to be the least among all the
26 studied architectures. This suggests that a trade-off, between the required ultimate strength from
27 one side and the progressive damage and toughness from the other side, has to be always
28 carefully considered.
29
30
31
32
33
34
35
36
37
38
39
40
41
42
43

44 **4.2.2 Failure analysis**

45
46 The difference in the final failure between the single and the multiple impact cases is
47 summarized in Fig. 12. The ASTM D7137 standard defines a three-letter code to describe the
48 failure mode. The first letter corresponds to the failure type; the second corresponds to the failure
49 area, and the third describes the failure location. In the case of single impact, the damage is so
50 localized and it does not cause the specimen to break in the middle. As per the standard, this
51 gauge failure (away from the induced damage due to impact) is still considered an acceptable
52 failure. The designated failure code for this case is LGM where L stands for lateral failure; G is
53 gauge/away from damage failure area, and M is the middle location. This gauge failure indicates
54
55
56
57
58
59
60
61
62
63
64
65

1
2
3
4 that the tested specimen is not sensitive to the induced damage, such that it fails at a compressive
5 stress close to the undamaged compressive strength. However, as previously noted in the case of
6 NCF and 2D-PW, the compressive strength due to single impact was relatively less than the
7 baseline counterparts. On the other hand, all the multiple-impacted specimens fail in the middle
8 along the impact horizontal line. The three-letter failure code for this case is LDM; where D
9 corresponds to at/through damage failure area. This, as per the ASTM standard, is again an
10 acceptable failure mode, and it provides a true measurement of the residual strength of the
11 specimens for the damage-induced state.
12
13
14
15
16
17
18
19

20 In order to further understand the damage progression, leading to the final failure of the
21 CAI specimens, DIC images were analyzed. The sequence of damage occurrence among the
22 three impacts is found to be the same for all the specimens regardless of their architecture. Thus,
23 Fig. 13 represents one example “ORT-PW” for illustration. Due to the boundary conditions of
24 the CAI fixture constraining the specimens’ edges, the damage initiates at the side impact
25 locations almost symmetrically. Upon load increase, the damage from the side impact grows
26 towards the central impact. Finally, the three impacted regions are connected as the damage
27 spans the full width of the specimen.
28
29
30
31
32
33
34
35

36 **5 Conclusion**

37
38
39 A systematic comparison of the impact resistance and damage tolerance of single vs.
40 multiple impacted NCF, 2D-PW, ORT-PW and ORT-TW composites was reported. All
41 specimens were impacted with 15 J and the damage tolerance was assessed using CAI testing.
42 The main difference between the ORT-PW and ORT-TW 3D woven architectures is the binder
43 frequency and the unit-cell size. It was observed that regardless of the unit-cell size, 3D woven
44 composites are more damage and delamination resistant to the transverse impact loading
45 compared to their 2D counterparts “NCF and 2D-PW”. In addition, the smaller the unit-cell size
46 is, the less damage the same impact energy causes. The load-displacement response of the
47 baseline specimens, loaded in compression, revealed the clear effect of crimp on the maximum
48 compressive strength. NCF had the maximum strength followed by 2D-PW, then ORT-TW and
49 the least being ORT-PW. The effect of the through-thickness binding yarns, on the buckling and
50 damage progression in compression, was captured by the difference between the NCF and 2D-
51
52
53
54
55
56
57
58
59
60
61
62
63
64
65

1
2
3
4 PW catastrophic failure from one side as opposed to the progressive gradual failure in the case of
5
6 3D woven composites. The reduction in CAI residual strength was minimal (~8%) in the case of
7
8 3D woven composites, followed by the 2D woven composites (~35%) and maximum in the case
9
10 of NCF composites (~45%). Finally, C-scanning, X-ray CT and DIC techniques were
11
12 successfully employed as NDT techniques to analyze and capture the effect of impact loading
13
14 and BVID on the different composite architectures in this study, which is quite essential in real
15
16 life applications so that the BVID does not go undetected.
17
18

19 **Acknowledgments**

20
21 Authors would like to acknowledge the CLSP (Composites Large Scale Project) UK Catapult
22
23 partners: Advanced Manufacturing Research Centre (AMRC), National Composite Centre
24
25 (NCC), Warwick Manufacturing Group (WMG) and Manufacturing Technology Centre (MTC)
26
27 for supporting this research.
28
29
30
31
32
33
34
35
36
37
38
39
40
41
42
43
44
45
46
47
48
49
50
51
52
53
54
55
56
57
58
59
60
61
62
63
64
65

References

- [1] Vogelesang LB, Vlot A. Development of fibre metal laminates for advanced aerospace structures. *J Mater Process Technol* 2000;103:1–5. doi:10.1016/S0924-0136(00)00411-8.
- [2] Castellanos AG, Prabhakar P. Durability and failure mechanics of woven carbon composites under repeated impact loading in Arctic conditions. *Multiscale Multidiscip Model Exp Des* 2018;1:157–70. doi:10.1007/s41939-018-0024-x.
- [3] Demirbrahim, Sayman O, Dogan A, Arikan V, Arman Y. The effects of repeated transverse impact load on the burst pressure of composite pressure vessel. *Compos Part B Eng* 2015;68:121–5. doi:10.1016/j.compositesb.2014.08.038.
- [4] Richardson MOW, Wisheart MJ. Review of low-velocity impact properties of composite materials. *Compos Part A Appl Sci Manuf* 1996;27:1123–31. doi:10.1016/1359-835X(96)00074-7.
- [5] Hao A, Sun B, Qiu Y, Gu B. Dynamic properties of 3-D orthogonal woven composite T-beam under transverse impact. *Compos Part A Appl Sci Manuf* 2008;39:1073–82. doi:10.1016/j.compositesa.2008.04.012.
- [6] Ji C, Sun B, Qiu Y, Gu B. Impact damage of 3D orthogonal woven composite circular plates. *Appl Compos Mater* 2007;14:343–62. doi:10.1007/s10443-008-9050-x.
- [7] Luo Y, Lv L, Sun B, Qiu Y, Gu B. Transverse impact behavior and energy absorption of three-dimensional orthogonal hybrid woven composites. *Compos Struct* 2007;81:202–9. doi:10.1016/j.compstruct.2006.08.011.
- [8] Seltzer R, González C, Muñoz R, Llorca J, Blanco-Varela T. X-ray microtomography analysis of the damage micromechanisms in 3D woven composites under low-velocity impact. *Compos Part A Appl Sci Manuf* 2013;45:49–60. doi:10.1016/j.compositesa.2012.09.017.
- [9] Gerlach R, Siviour CR, Wiegand J, Petrinic N. In-plane and through-thickness properties, failure modes, damage and delamination in 3D woven carbon fibre composites subjected to impact loading. *Compos Sci Technol* 2012;72:397–411. doi:10.1016/j.compscitech.2011.11.032.
- [10] Mouritz AP, Bannister MK, Falzon PJ, Leong KH. Review of applications for advanced three-dimensional fibre textile composites. *Compos Part A* 1999;30:1445–61.
- [11] Shah SZH, Karuppanan S, Megat-Yusoff PSM, Sajid Z. Impact resistance and damage tolerance of fiber reinforced composites: A Review. *Compos Struct* 2019;217:100–21. doi:10.1016/J.COMPSTRUCT.2019.03.021.
- [12] El-Dessouky HM, Saleh MN. Chapter 4: 3D Woven Composites: From Weaving to Manufacturing. *Recent Dev. F. Carbon Fibers*, IntechOpen; 2018, p. 51–66. doi:10.5772/intechopen.74311.
- [13] Greve L, Pickett AK. Delamination testing and modelling for composite crash simulation. *Compos Sci Technol* 2006;66:816–26. doi:10.1016/j.compscitech.2004.12.042.
- [14] Hart KR, Chia PXL, Sheridan LE, Wetzel ED, Sottos NR, White SR. Mechanisms and characterization of impact damage in 2D and 3D woven fiber-reinforced composites. *Compos Part A Appl Sci Manuf* 2017;101:432–43. doi:10.1016/j.compositesa.2017.07.004.
- [15] Sottos NR, Chia PXL, Hart KR, Sheridan LE, White SR, Wetzel ED. Comparison of

- 1
2
3
4 Compression-After-Impact and Flexure-After-Impact protocols for 2D and 3D woven fiber-
5 reinforced composites. *Compos Part A Appl Sci Manuf* 2017;101:471–9.
6 doi:10.1016/j.compositesa.2017.07.005.
7
- 8 [16] González E V., Maimí P, Camanho PP, Turon A, Mayugo JA. Simulation of drop-weight impact
9 and compression after impact tests on composite laminates. *Compos Struct* 2012;94:3364–78.
10 doi:10.1016/j.compstruct.2012.05.015.
11
- 12 [17] Jang BZ, Chen LC, Wang CZ, Lin HT, Zee RH. Impact resistance and energy absorption
13 mechanisms in hybrid composites. *Compos Sci Technol* 1989;34:305–35. doi:10.1016/0266-
14 3538(89)90002-X.
15
- 16 [18] Wang M, Cao M, Wang H, Siddique A, Gu B, Sun B. Drop-weight impact behaviors of 3-D angle
17 interlock woven composites after thermal oxidative aging. *Compos Struct* 2017;166:239–55.
18 doi:10.1016/j.compstruct.2017.01.046.
19
- 20 [19] Potluri P, Hogg P, Arshad M, Jetavat D, Jamshidi P. Influence of fibre architecture on impact
21 damage tolerance in 3D woven composites. *Appl Compos Mater* 2012;19:799–812.
22 doi:10.1007/s10443-012-9256-9.
23
- 24 [20] Chen F, Hodgkinson JM. Impact behaviour of composites with different fibre architecture. *Proc*
25 *Inst Mech Eng Part G J Aersp Eng* 2009;223:1009–17. doi:10.1243/09544100JAERO451.
26
- 27 [21] Huang CT, Jang BP, Kowbel W, Hsieh CY, Jang BZ. Repeated Impact Failure of Continuous
28 Fiber Reinforced Thermoplastic and Thermoset Composites. *J Compos Mater* 2017;25:1171–203.
29 doi:10.1177/002199839102500906.
30
- 31 [22] BIENIAŚ J, SUROWSKA B, JAKUBCZAK P. Influence of repeated impact on damage growth in
32 fibre reinforced polymer composites. *Ekspluat i Niezawodn - Maint Reliab* 2015;17:194–8.
33 doi:10.17531/ein.2015.2.4.
34
- 35 [23] Rotem A. The Strength of Laminated Composite Materials Under Repeated Impact Loading.
36 *Compos Technol Res* 1988;10:74–9.
37
- 38 [24] Baucom JN, Zikry MA, Rajendran AM. Low-velocity impact damage accumulation in woven S2-
39 glass composite systems. *Compos Sci Technol* 2006;66:1229–38.
40 doi:10.1016/j.compscitech.2005.11.005.
41
- 42 [25] ASTM D7136/D7136M-15 Standard Test Method for Measuring the Damage Resistance of a
43 Fiber-Reinforced Polymer Matrix Composite to a Drop-Weight Impact Event 2011;i:1–16.
44 doi:10.1520/D7136.
45
- 46 [26] ASTM D7137/D7137M-12 Standard Test Method for Compressive Residual Strength Properties
47 of Damaged Polymer Matrix Composite Plates. *Annu B ASTM Stand* 2012;i:1–17.
48 doi:10.1520/D7137.
49
- 50 [27] Mubeen A. Damage Tolerance of 3D Woven Composites with Weft Binders. The University of
51 Manchester, 2014. doi:10.1002/ejoc.201200111.
52
- 53 [28] Saleh MN, Yudhanto A, Potluri P, Lubineau G, Soutis C. Characterising the loading direction
54 sensitivity of 3D woven composites: Effect of z-binder architecture. *Compos Part A Appl Sci*
55 *Manuf* 2016;90:577–88. doi:10.1016/j.compositesa.2016.08.028.
56
- 57 [29] Saleh MN, Soutis C. Recent advancements in mechanical characterisation of 3D woven
58
59
60
61
62
63
64
65

- 1
2
3
4 composites. *Mech Adv Mater Mod Process* 2017;3. doi:10.1186/s40759-017-0027-z.
5
- 6 [30] Saleh MN, Wang Y, Yudhanto A, Joesbury A, Potluri P, Lubineau G, et al. Investigating the
7 Potential of Using Off-Axis 3D Woven Composites in Composite Joints' Applications. *Appl*
8 *Compos Mater* 2016;24:377–96. doi:10.1007/s10443-016-9529-9.
9
- 10 [31] Ivanov DS, Lomov S V., Bogdanovich AE, Karahan M, Verpoest I. A comparative study of tensile
11 properties of non-crimp 3D orthogonal weave and multi-layer plain weave E-glass composites.
12 Part 2: Comprehensive experimental results. *Compos Part A Appl Sci Manuf* 2009;40:1144–57.
13 doi:10.1016/j.compositesa.2009.04.032.
14
- 15 [32] Dai S, Cunningham PR, Marshall S, Silva C. Open hole quasi-static and fatigue characterisation of
16 3D woven composites. *Compos Struct* 2015;131:765–74. doi:10.1016/j.compstruct.2015.06.032.
17
- 18 [33] Midani M, Seyam A-F, Saleh MN, Pankow M. The effect of the through-thickness yarn
19 component on the in-and out-of-plane properties of composites from 3D orthogonal woven
20 preforms. *J Text Inst* 2018. doi:10.1080/00405000.2018.1481722.
21
- 22 [34] Saleh MN, Lubineau G, Potluri P, Withers PJ, Soutis C. Micro-mechanics based damage
23 mechanics for 3D orthogonal woven composites: Experiment and numerical modelling. *Compos*
24 *Struct* 2016;156:115–214. doi:10.1016/j.compstruct.2016.01.021.
25
- 26 [35] Lomov S V., Bogdanovich AE, Ivanov DS, Mungalov D, Karahan M, Verpoest I. A comparative
27 study of tensile properties of non-crimp 3D orthogonal weave and multi-layer plain weave E-glass
28 composites. Part 1: Materials, methods and principal results. *Compos Part A Appl Sci Manuf*
29 2009;40:1134–43. doi:10.1016/j.compositesa.2009.04.032.
30
- 31 [36] L. Tong, A.P. Mouritz MB. Chapter 5 3D Woven Composites. *3D Fibre Reinf. Polym. Compos.*,
32 2009.
33
- 34 [37] Cox BN, Dadkhah MS, Inman R V, Morris WL, Zupon J, International R, et al. Mechanisms of
35 Compressive Failure in 3D Composites. *Acta Metall Mater* 1992;40:3285–98.
36
- 37 [38] Wang Y. Effect of Fabric Structures on the Mechanical Properties of 3-D Textile Composites. *J*
38 *Ind Text* 2006;35:239–56. doi:10.1177/1528083706057595.
39
- 40 [39] Gerlach R, Siviour CR, Wiegand J, Petrinic N. In-plane and through-thickness properties, failure
41 modes, damage and delamination in 3D woven carbon fibre composites subjected to impact
42 loading. *Compos Sci Technol* 2012;72:397–411. doi:10.1016/j.compscitech.2011.11.032.
43
- 44 [40] Stig F, Hallström S. Influence of crimp on 3D-woven fibre reinforced composites. *Compos Struct*
45 2013;95:114–22. doi:10.1016/j.compstruct.2012.07.022.
46
- 47 [41] Saleh MN, Yudhanto A, Lubineau G, Soutis C. The effect of z-binding yarns on the electrical
48 properties of 3D woven composites. *Compos Struct* 2017;182:606–16.
49 doi:10.1016/j.compstruct.2017.09.081.
50
51
52
53
54
55
56
57
58
59
60
61
62
63
64
65

1
2
3
4 **List of Figures**
5

6 Fig. 1. Schematic of the different types of investigated composites: a) NCF, b) 2D-PW, c) ORT-
7 PW and d) ORT-TW (The warp yarns highlighted in blue, the weft yarns in grey, the through
8 thickness binders in red, and the stitch yarns for the non-crimp fabric (NCF) in green) **Error!**
9

10 **Bookmark not defined.**
11

12 Fig. 2. Schematic of: a) Single-impacted and b) Multiple-impacted specimens (dimensions in
13 mm).....**Error! Bookmark not defined.**
14

15 Fig. 3. Testing setup: a) First impact, b) Second impact, c) Third impact and d) CAI **Error!**
16

17 **Bookmark not defined.**
18

19 Fig. 4. C-scanning and DIC results for single-impacted specimens**Error! Bookmark not**
20 **defined.**
21

22 Fig. 5. C-scanning and DIC results for multiple-impacted specimens**Error! Bookmark not**
23 **defined.**
24

25 Fig. 6. Impact load-displacement curves for: a) NCF, b) 2D-PW, c) ORT-PW and d) ORT-TW
26**Error! Bookmark not defined.**
27

28 Fig. 7. Single vs. multiple impact: a) C-scan impacted area and b) Energy absorption **Error!**
29 **Bookmark not defined.**
30

31 Fig. 8. X-ray CT cross-sections after impact for: a) NCF, b) 2D-PW, c) ORT-PW and d) ORT-
32 TW**Error! Bookmark not defined.**
33

34 Fig. 9. Dent depth measured by the DIC: a) Single and b) Multiple impact**Error! Bookmark not**
35 **defined.**
36

37 Fig. 10. Summary of the load-displacement curves for: a) Baseline, b) Single impact, c) Multiple
38 impact and d) Residual strength for all the tested architectures**Error! Bookmark not defined.**
39

40 Fig. 11. Schematic of kink band formation: a) 2D laminates, b) 3D woven composites **Error!**
41 **Bookmark not defined.**
42

43 Fig. 12. Comparison of failure of: a) Single impact and b) Multiple impact specimens for all
44 architectures**Error! Bookmark not defined.**
45

46 Fig. 13. Representative damage progression in CAI: a) Side impacts damage, b) Damage growth
47 from the edges to the central impact; c) Damage spans the full width of the specimen..... **Error!**
48

49 **Bookmark not defined.**
50
51
52
53
54
55
56
57
58
59
60
61
62
63
64
65

1
2
3
4
5
6
7
8
9
10
11
12
13
14
15
16
17
18
19
20
21
22
23
24
25
26
27
28
29
30
31
32
33
34
35
36
37
38
39
40
41
42
43
44
45
46
47
48
49
50
51
52
53
54
55
56
57
58
59
60
61
62
63
64
65

List of Tables

Table 1 Summary of the percentage of damaged area for single and multiple impacts **Error!**

Bookmark not defined.

Table 2 Maximum compressive force (kN) for baseline, single and multiple impact cases . **Error!**

Bookmark not defined.

Figure 1
[Click here to download high resolution image](#)

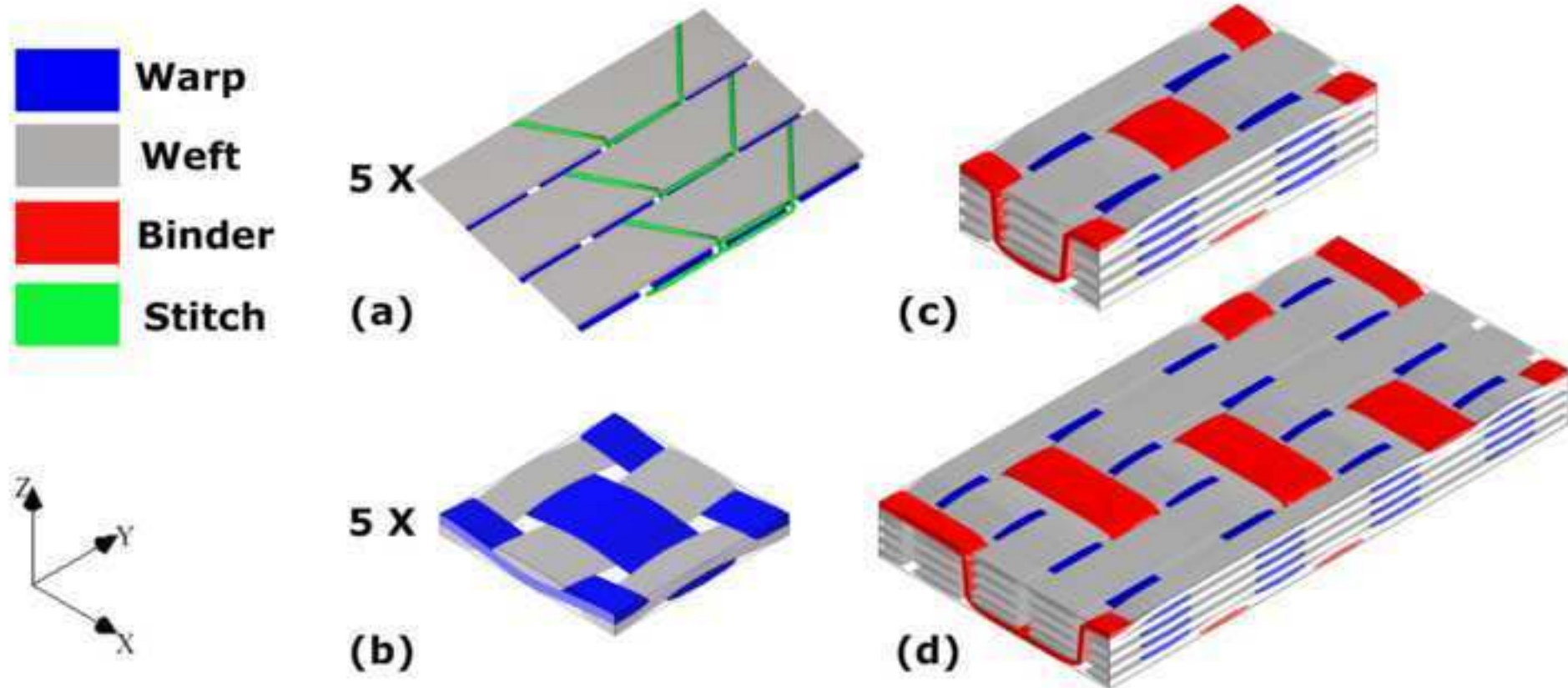


Figure 2
[Click here to download high resolution image](#)

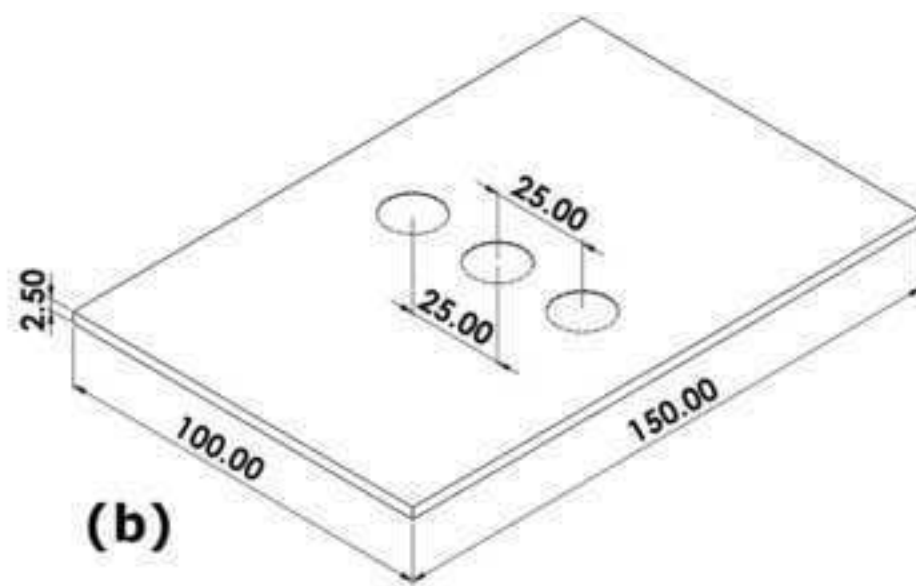
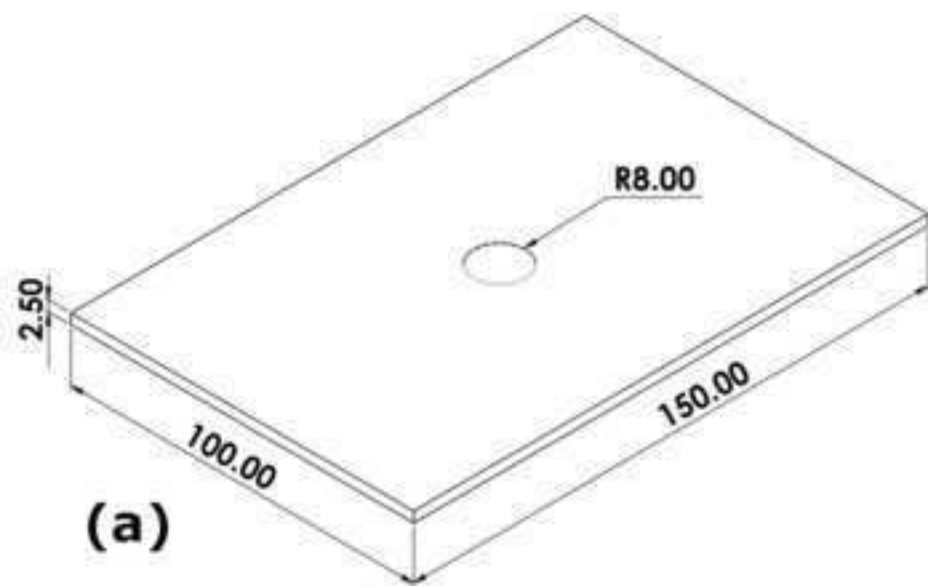


Figure 3
[Click here to download high resolution image](#)

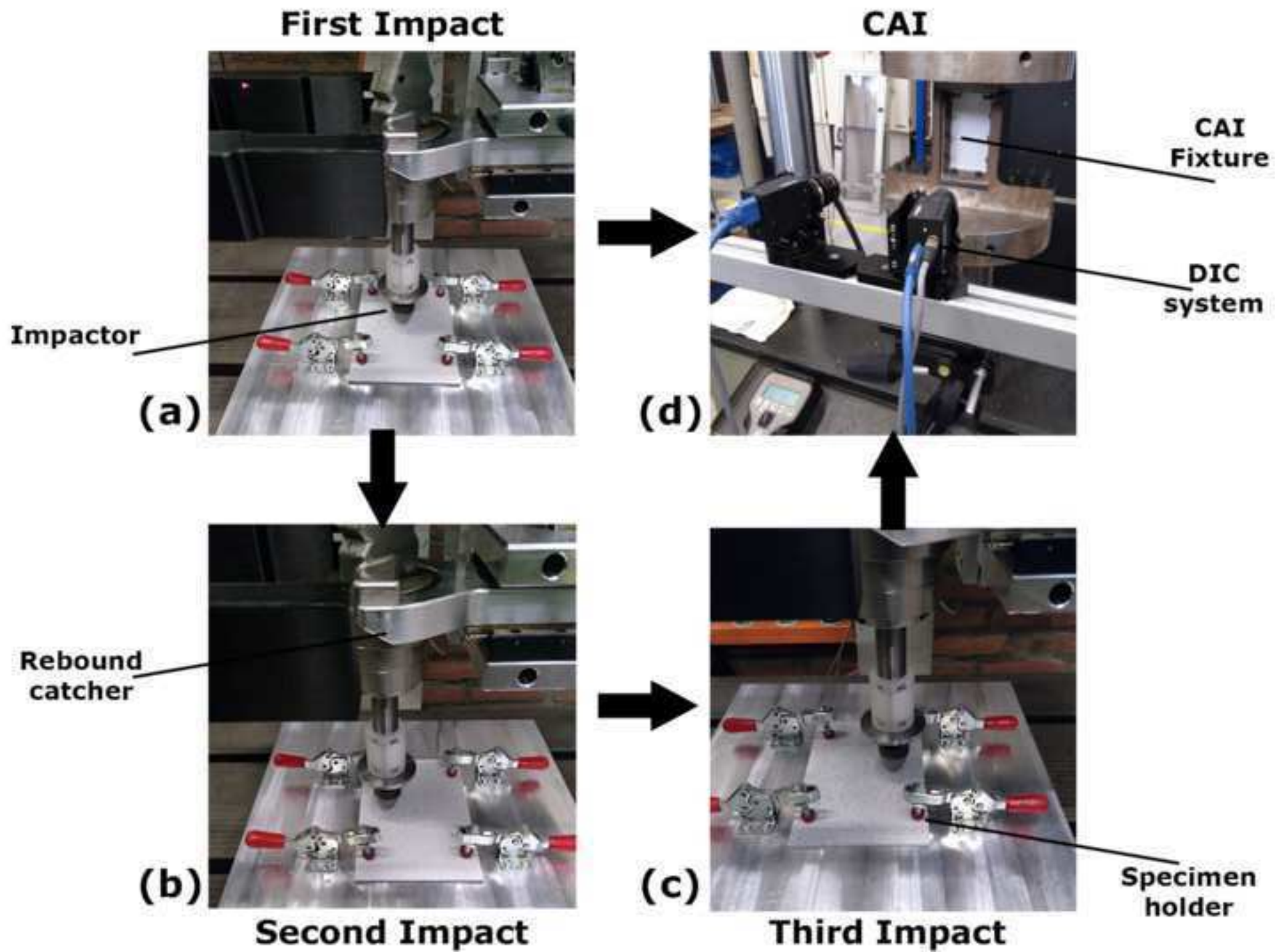


Figure 4
[Click here to download high resolution image](#)

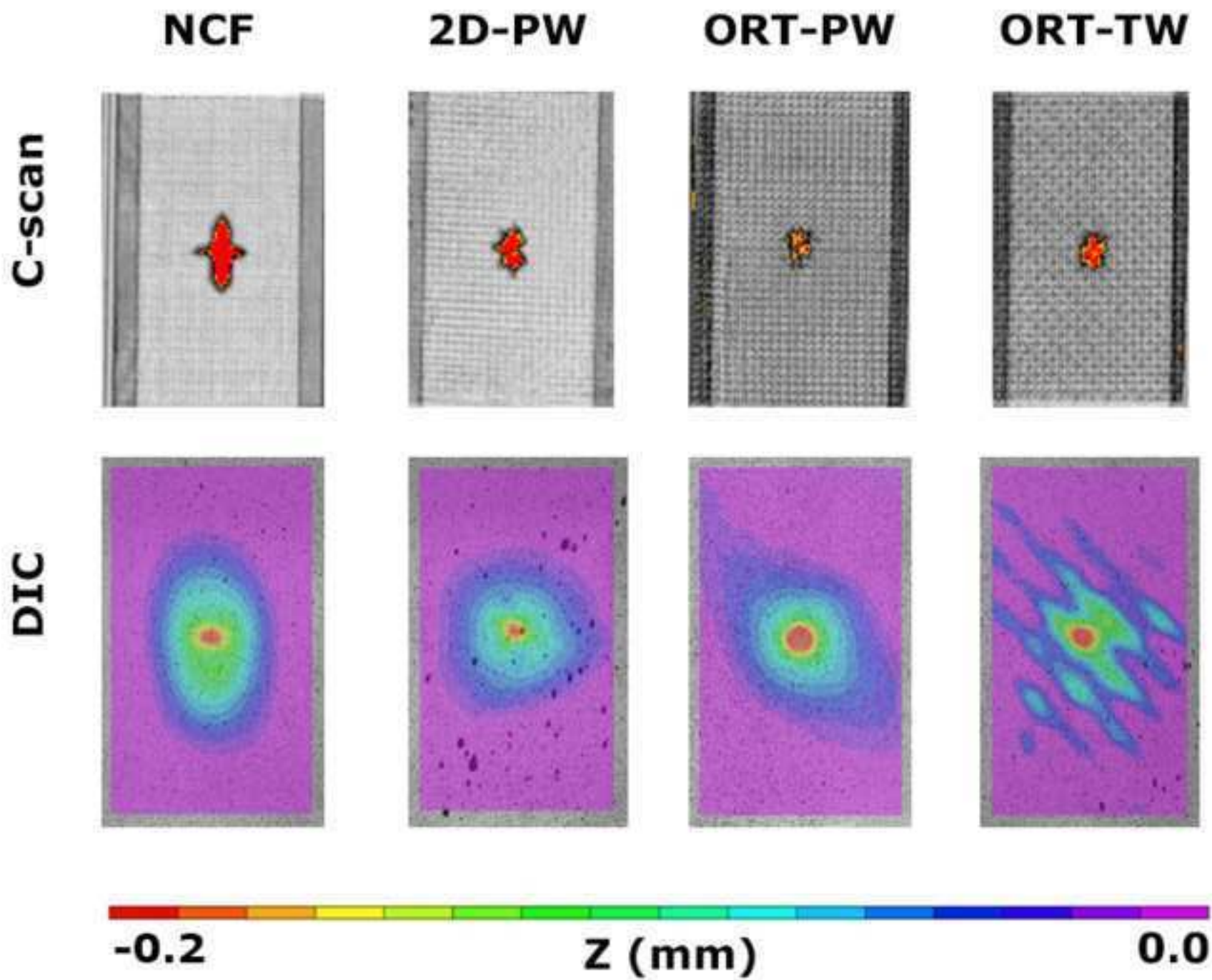


Figure 5
[Click here to download high resolution image](#)

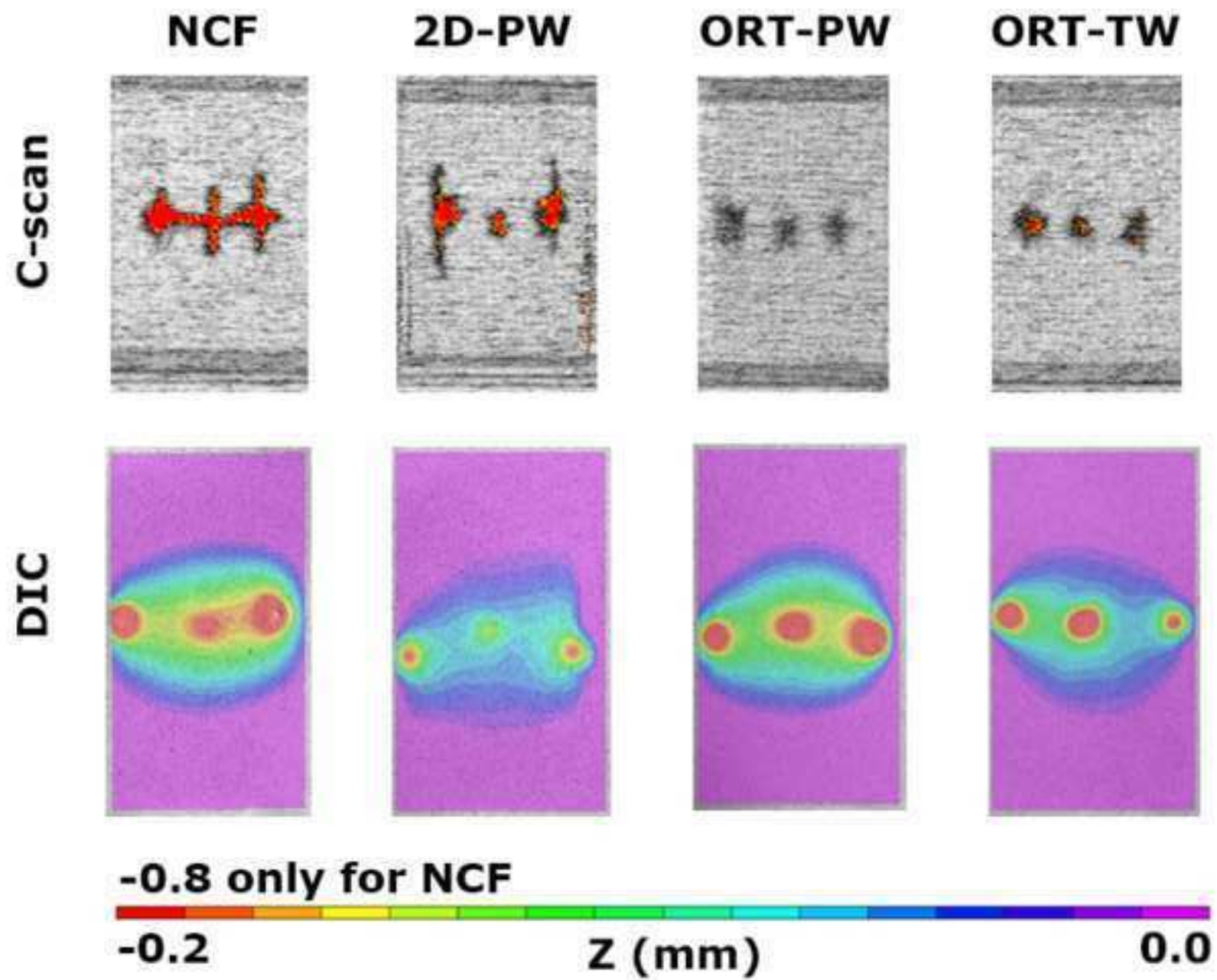


Figure 6
[Click here to download high resolution image](#)

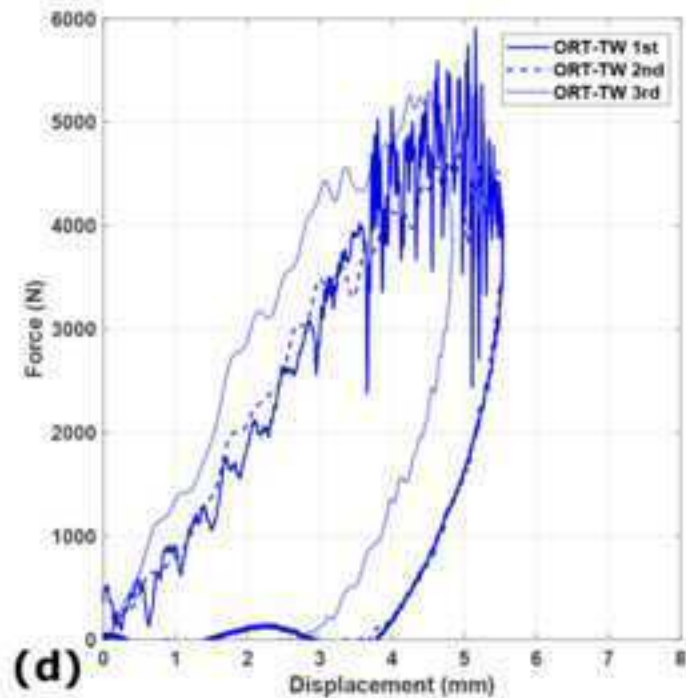
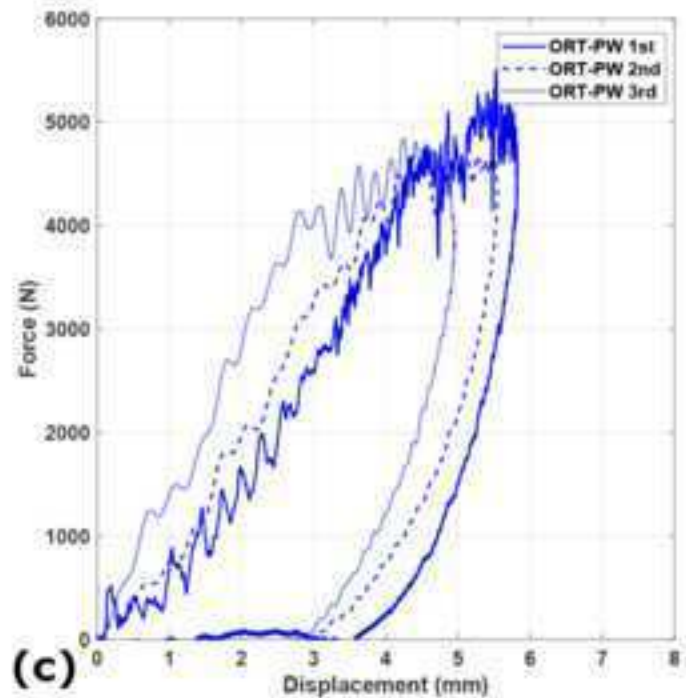
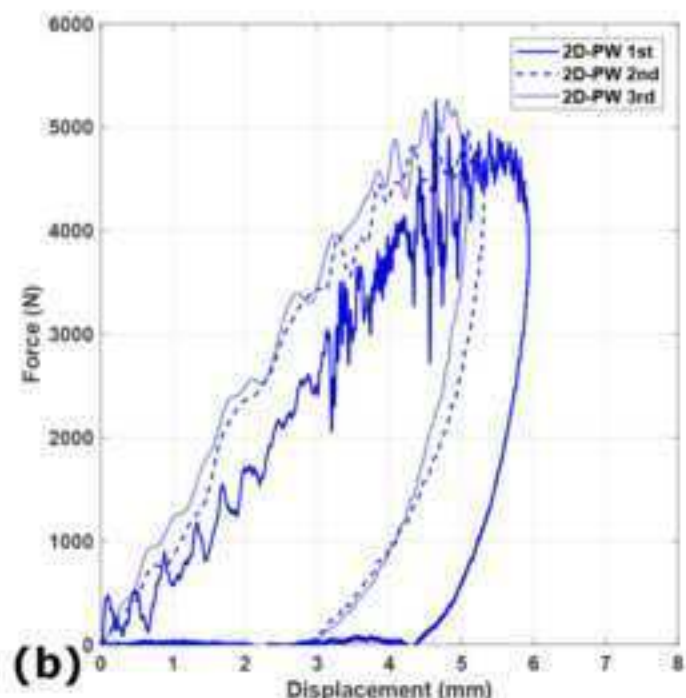
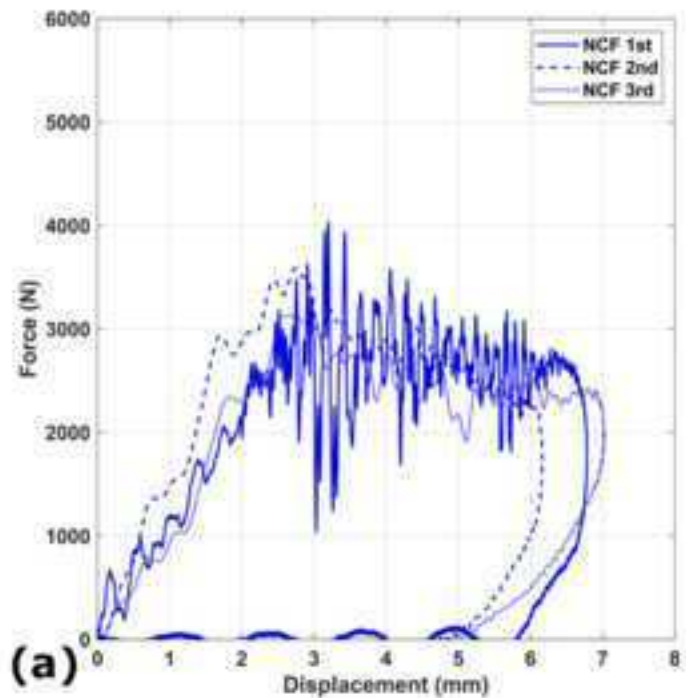


Figure 7
[Click here to download high resolution image](#)

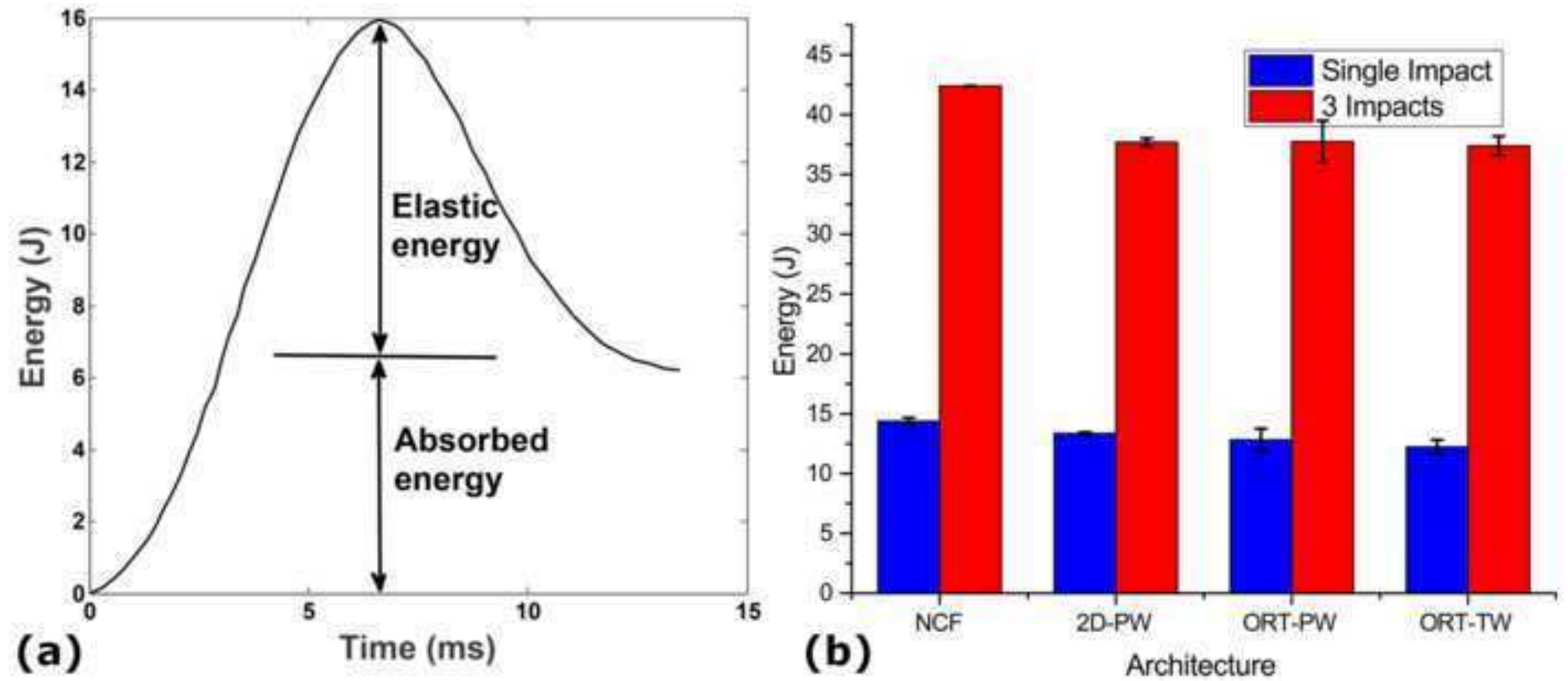


Figure 8
[Click here to download high resolution image](#)

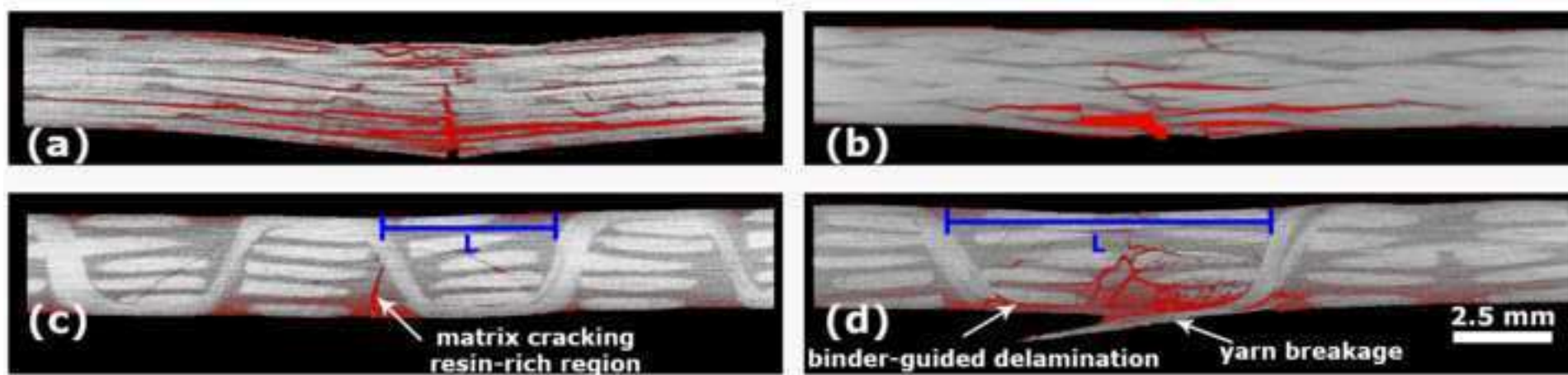


Figure 9
[Click here to download high resolution image](#)

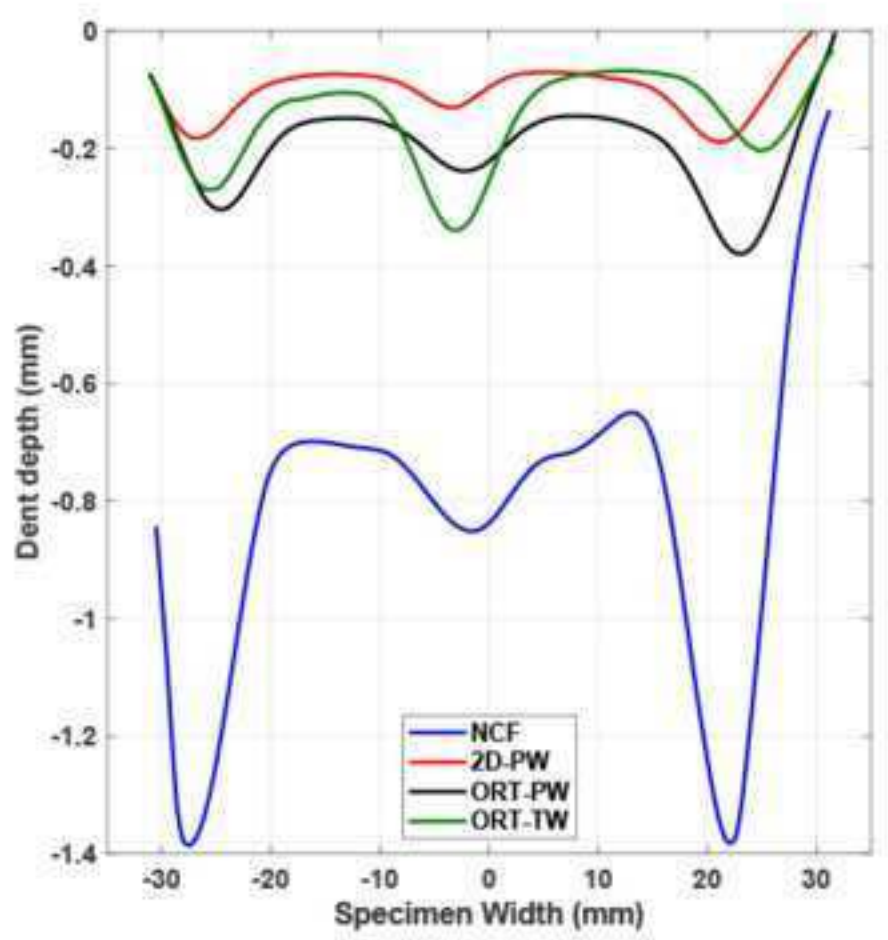
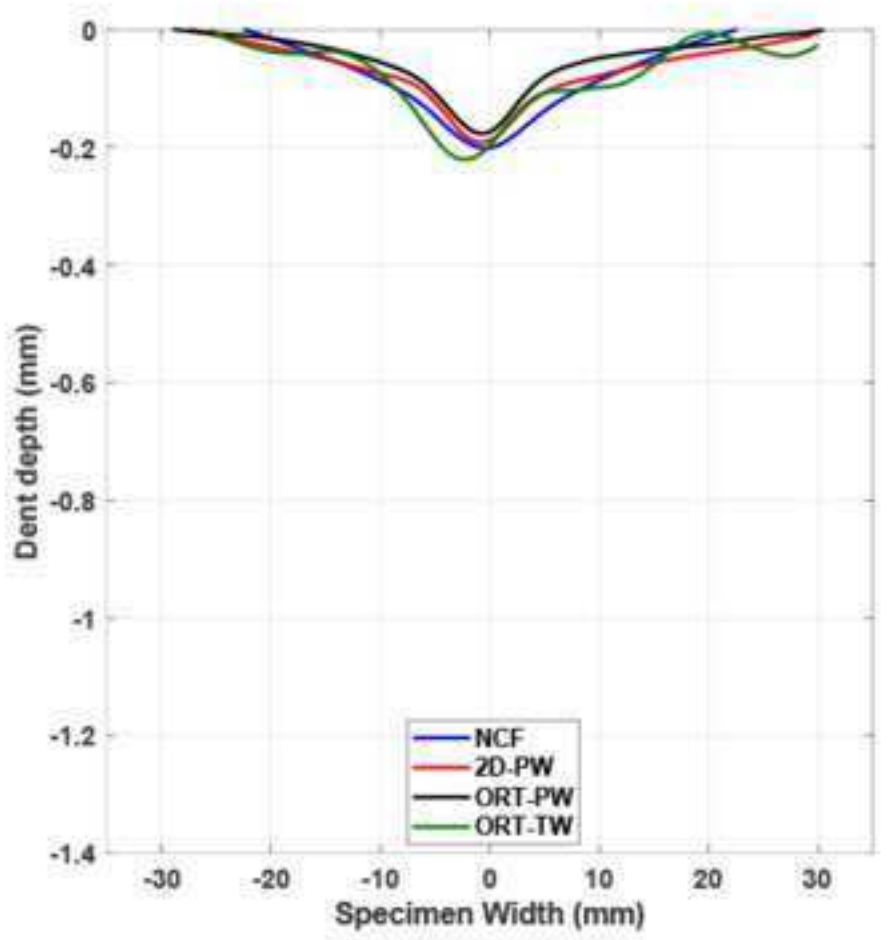
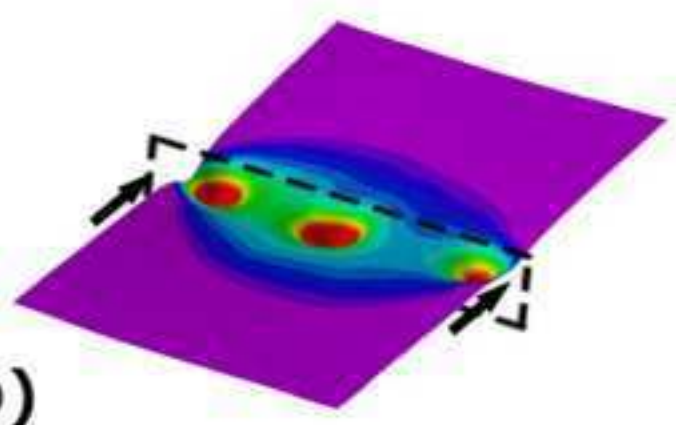
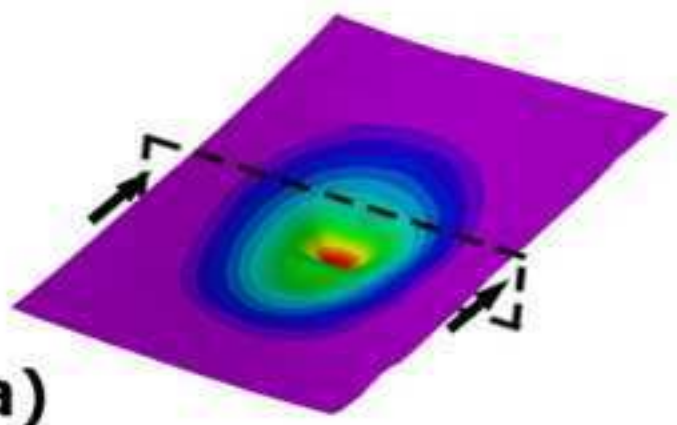
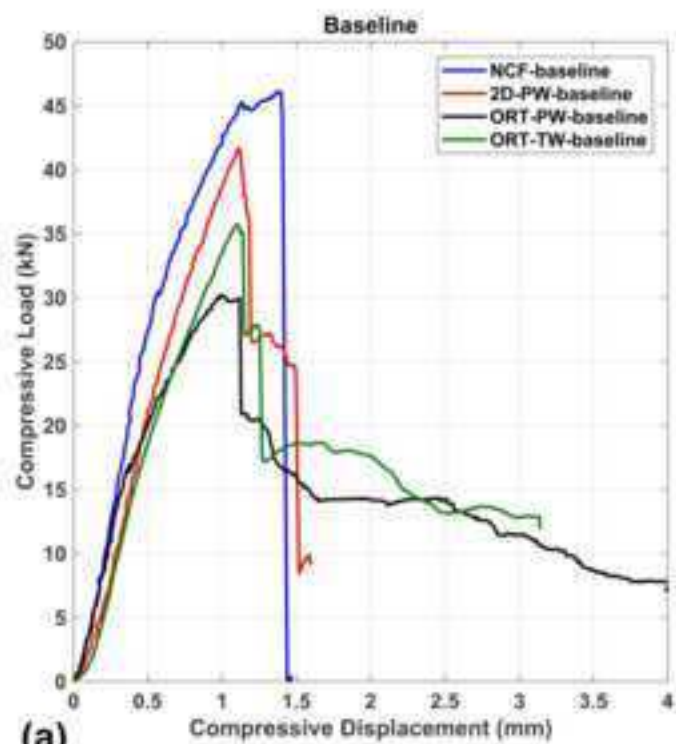
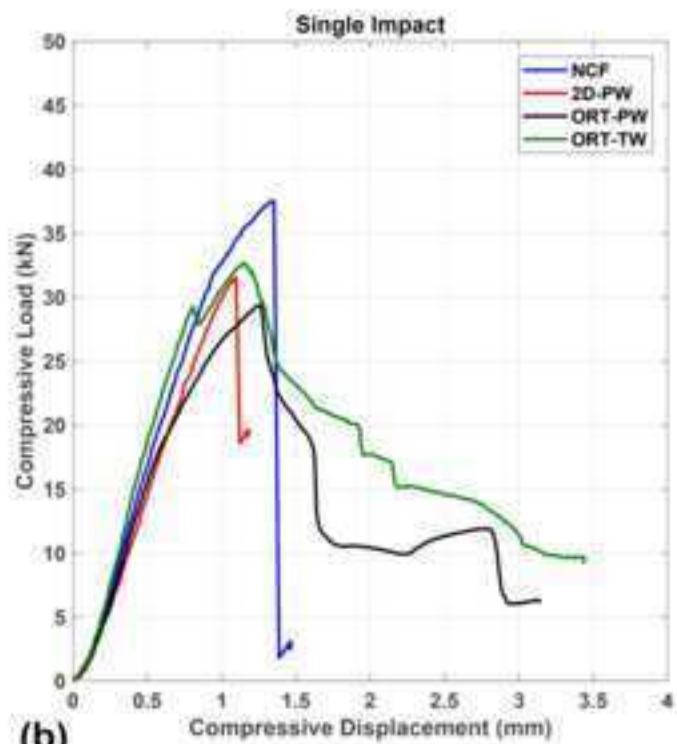


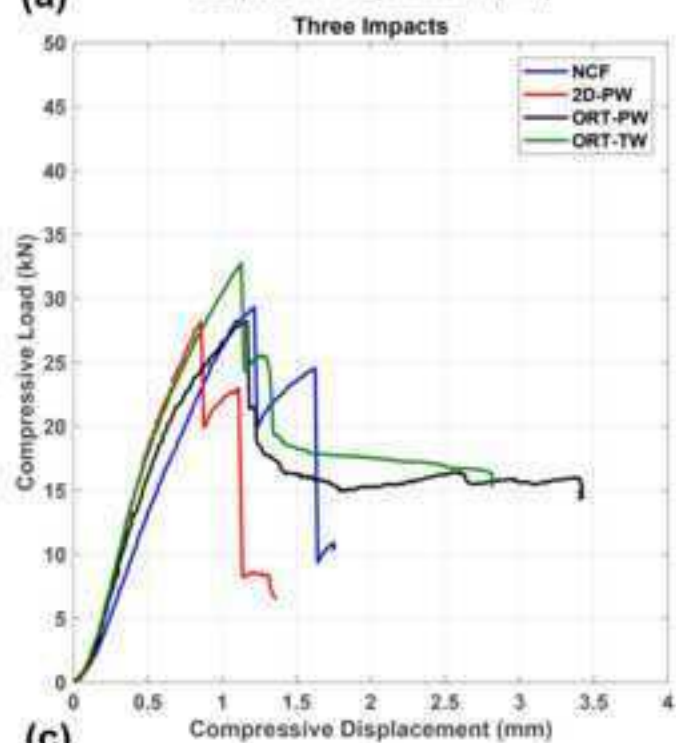
Figure 10
[Click here to download high resolution image](#)



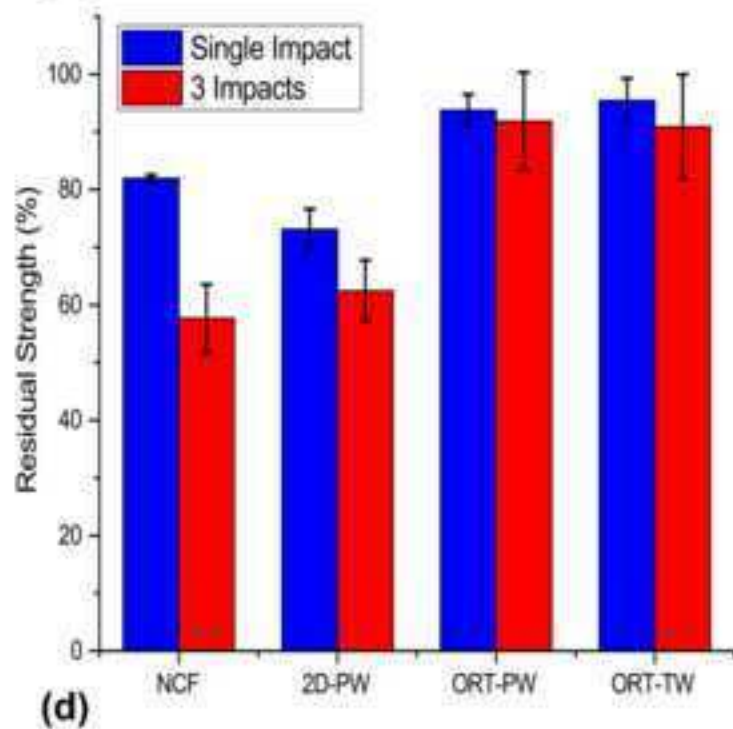
(a)



(b)



(c)



(d)

Figure 11
[Click here to download high resolution image](#)

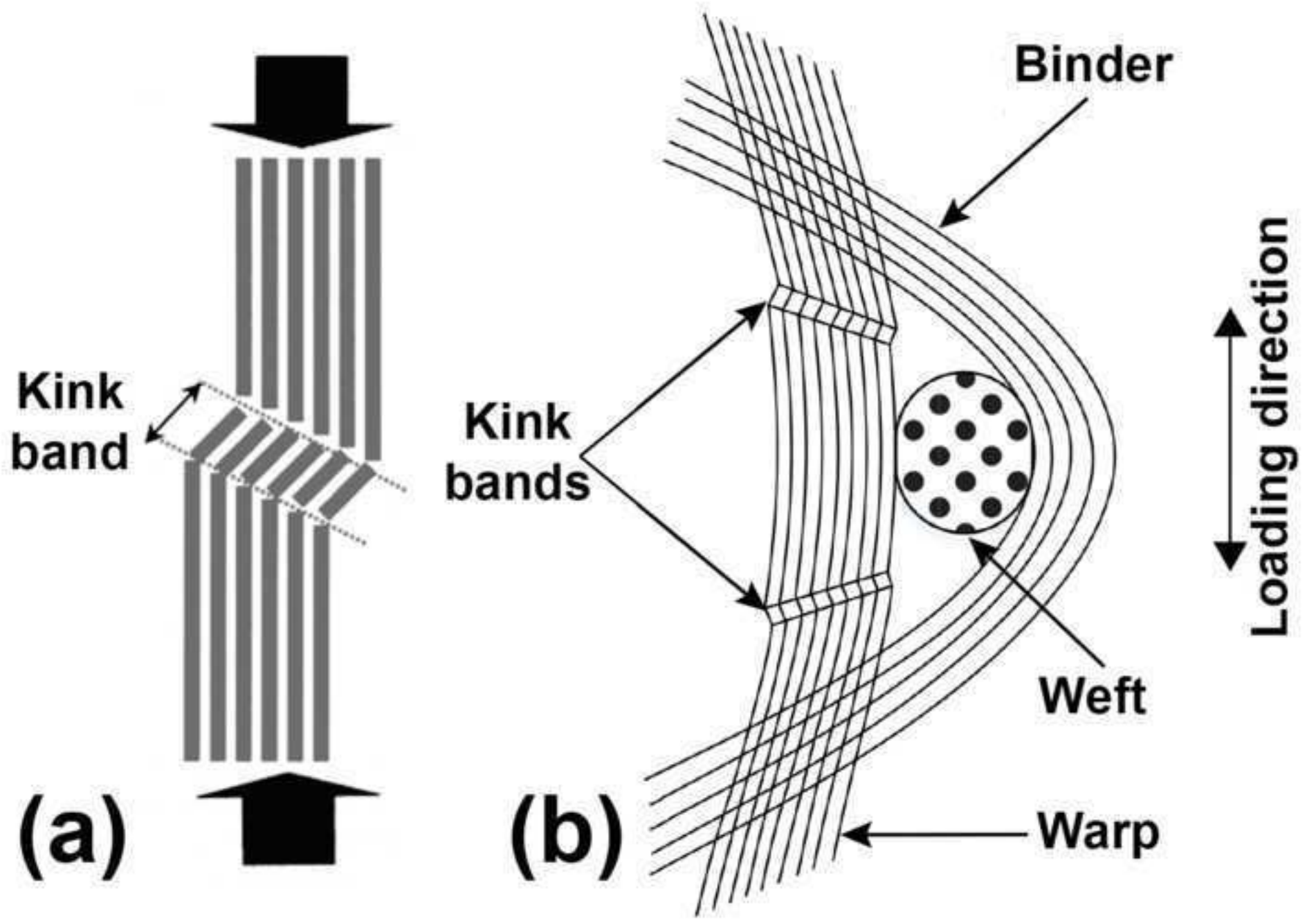


Figure 12
[Click here to download high resolution image](#)

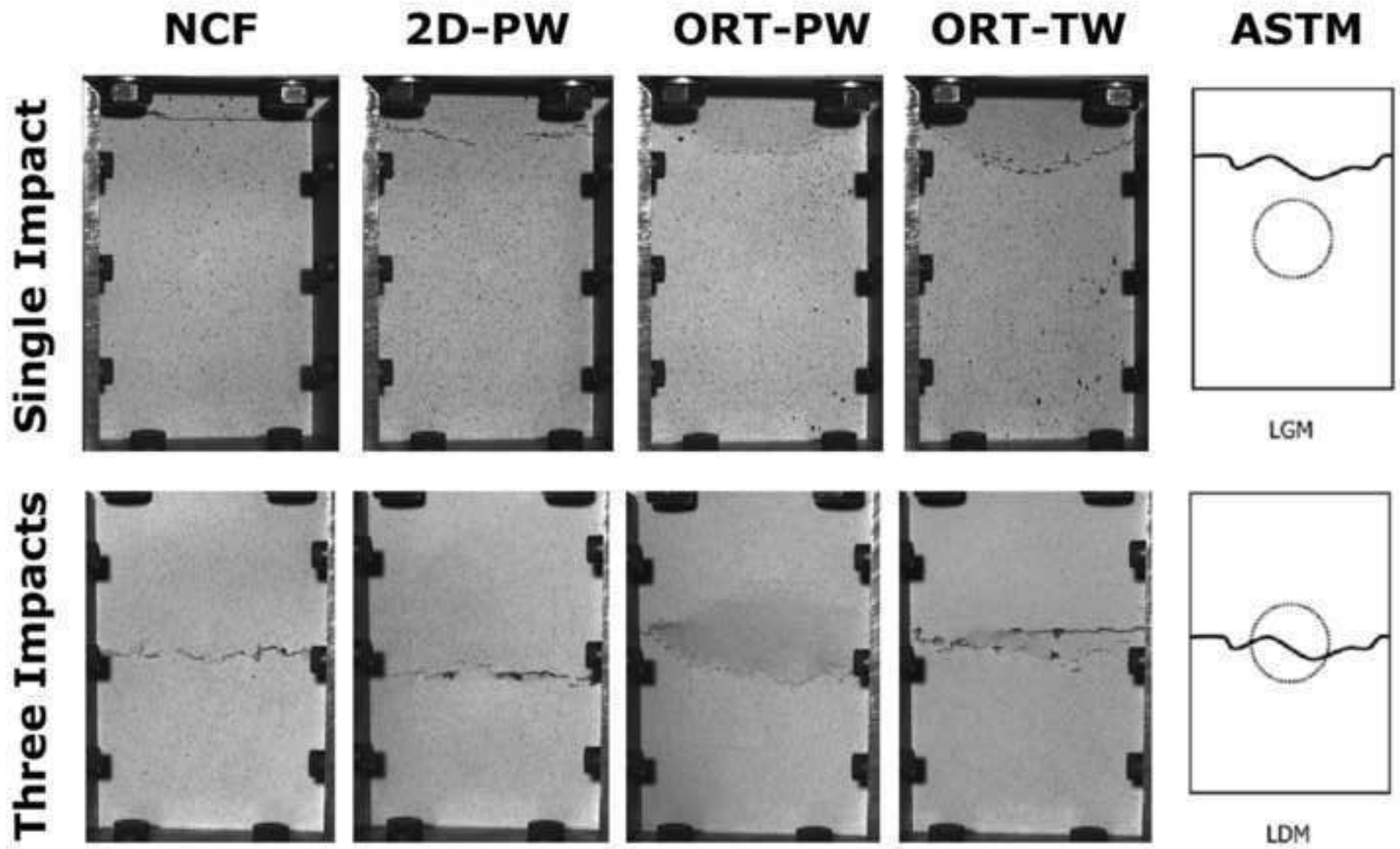


Figure 13
[Click here to download high resolution image](#)

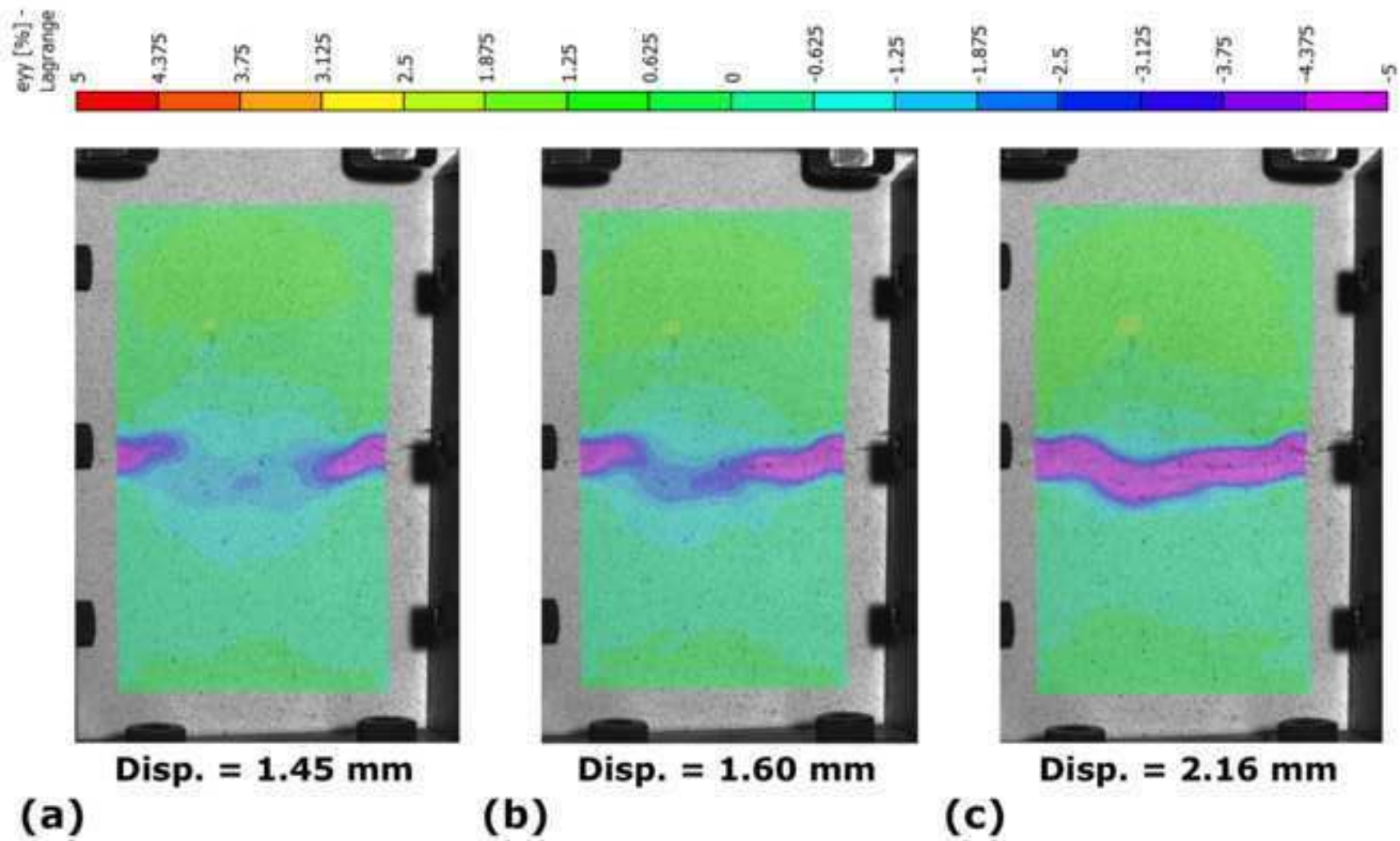


Table 1 Summary of the percentage of damaged area for single and multiple impacts

Architecture	Single Impact	Multiple Impacts
NCF	1.81 ± 0.29	4.01 ± 0.11
2D-PW	1.05 ± 0.12	2.35 ± 0.16
ORT-PW	0.66 ± 0.08	1.43 ± 0.27
ORT-TW	1.02 ± 0.03	1.88 ± 0.14

Table 2 Maximum compressive force (kN) for baseline, single and multiple impact cases

Architecture	Baseline	Single Impact	Multiple Impacts
NCF	46.11 ± 1.45	37.80 ± 0.27	26.59 ± 2.72
2D-PW	41.69 ± 1.85	30.49 ± 1.48	26.03 ± 2.22
ORT-PW	30.17 ± 1.69	28.29 ± 0.83	27.71 ± 2.57
ORT-TW	35.69 ± 2.30	34.06 ± 1.39	32.45 ± 3.24